Mechanisms of cilia regeneration in *Xenopus* multiciliated epithelium *in vivo*.

Venkatramanan G. Rao[1], Vignesharavind Subramanianbalachandar[1], Magdalena M. Magaj[1,3,4] Stefanie Redemann[1,3,4], Saurabh S. Kulkarni[1,2,3 *]

1- Department of Cell Biology, University of Virginia, Charlottesville, VA 22903
2- Department of Biology, University of Virginia, Charlottesville, VA 22903
3- Center for Membrane & Cell Physiology, University of Virginia, Charlottesville, VA 22903
4- Department of Molecular Physiology and Biological Physics, University of Virginia, Charlottesville, VA 22903

*- Author for correspondence (sk4xq@virginia.edu)

Keywords

Cilia, transition zone, regeneration, *Xenopus*, B9d1, central pair, cilia tip, IFT43, ciliogenesis, Sentan

SUMMARY

Cilia regeneration is a physiological event, and while studied extensively in unicellular organisms, it remains poorly understood in vertebrates. In this study, using *Xenopus* multiciliated cells (MCCs) as a model, we demonstrate that, unlike unicellular organisms, deciliation removes the transition zone (TZ) along with the ciliary axoneme. While MCCs immediately begin the regeneration of the ciliary axoneme, surprisingly, the assembly of TZ was delayed. Instead, ciliary tip proteins, Sentan and Clamp, were the first to localize to regenerating cilia. Using cycloheximide (CHX) to block new protein synthesis, we show that the TZ protein B9d1 is not a component of the cilia precursor pool and requires new transcription/translation providing insights into the delayed repair of TZ. Moreover, CHX treatment led MCCs to assemble fewer (~ ten compared to ~150 in controls) but about wild-type length (78% of WT) cilia by gradually concentrating ciliogenesis proteins like IFT43 at a select few basal bodies, highlighting the exciting possibility of protein transport between basal bodies to facilitate faster regeneration in cells with multiple cilia. In summary, we demonstrate that MCCs begin regeneration with the assembly of ciliary tip and axoneme followed by TZ, questioning the importance of TZ in motile ciliogenesis.

INTRODUCTION

Cilia perform critical functions as the signaling hub (primary cilia) and force generator to create extracellular fluid flow (motile cilia) during development. Dysfunction of cilia can manifest into a constellation of defects like polycystic kidney disease[1,2], congenital heart disease[1], primary ciliary dyskinesia[2], retinal degeneration, etc., known as ciliopathies[3]. Nevertheless, how cells assemble a cilium remains a central outstanding question in the field.

Cilium is an extracellular hairlike organelle composed of a microtubule-based cytoskeleton called the ciliary axoneme covered with a membrane[4]. Cilium is anchored to the cell via a basal body (modified centriole) and enclosed by a specialized plasma membrane domain[4,5]. The ciliary axoneme consists of the ciliary shaft and ciliary tip. The ciliary shaft is the main body of the axoneme and is made of 9+0 or 9+2 microtubule doublets in sensory or motile cilia, respectively[4]. The structure of the ciliary tip can vary across species and ciliary types; however, it usually is made of microtubule singlets in motile cilia[6,7]. Transition zone (TZ) is a structural junction between the basal body and the axoneme proposed to form a molecular sieve-like barrier[8,9]. It acts like a "ciliary gate" regulating intraciliary protein traffic[8,10,11]. In order to understand how cells construct such a complex structure, it is necessary to analyze the spatial and temporal order of the assembly of each component in the context of the entire cilium.

The common understanding in the field is that cilia assemble bottom-up from the basal body, followed by the TZ and then the ciliary shaft and ciliary tip, like constructing a tower. However, no direct evidence has been gathered because cilium assembly happens in the context of other intracellular events like basal body migration and cytoskeleton remodeling[12–14], making it challenging to tease out the spatial and temporal sequence of events. Alternatively, one can study ciliogenesis in a simpler model by removing mature cilia and observing the cells reassemble the entire structure without the confounding signals from basal body maturation or cytoskeleton remodeling[12,13,15]. While it is important to remember that regeneration of cilia may not be identical to *de novo* assembly, cilia regeneration studies in *Chlamydomonas reinhardtii* have provided significant insights into ciliogenesis, e.g., cargo transport, the presence of precursor pool, regulation of ciliary gene expression[15–17]

The deciliation-regeneration approach offers clear advantages to understanding ciliogenesis. However, in vertebrates, this has been hindered by a few challenges. First, multiciliated cells

(MCCs) are often present in tissues (ependymal cells in the brain and multiciliated cells in the lungs), are not accessible for inducing controlled deciliation, and offer technical challenges to studying regeneration by imaging. The use of cell culture could circumvent this challenge. However, a detailed study in which primary cilia or MCCs have been deciliated and regenerated is absent in the literature. However, these obstacles can be overcome by studying MCCs of the *Xenopus* embryonic epidermis. Previous studies have demonstrated that *Xenopus* multiciliated epithelium can be deciliated using the Ca^{2+} shock in an *in vivo* setting, and these cilia regenerate within hours [18–20]. Using this *in vivo* vertebrate system of deciliation and regeneration of cilia, we explored the fundamental questions of spatial and temporal dynamics of cilia assembly.

RESULTS AND DISCUSSION

Cilia regeneration on *Xenopus* mucociliary epithelium

The MCCs of the *Xenopus* embryonic epidermis were consistently deciliated within 10-15 seconds of exposure to a deciliation buffer, as confirmed by the loss of acetylated (Ac.) α-tubulin signal (**Fig. 1A-B**). The recovery of Ac. α-tubulin signal was observed within an hour, indicating the initiation of cilia regeneration, with cilia reaching wild-type length by 6 hours (Fig. 1C). Compared to *Chlamydomonas*, where both cilia can attain full length in 90 minutes, the regeneration of cilia in MCCs of *Xenopus* takes longer, raising interesting questions about the underlying mechanisms. One possibility is that the delay in cilia regeneration in MCCs may be due to the requirement to reassemble hundreds of cilia instead of just two in *Chlamydomonas*. Alternatively, the entire MCC may be replaced by a stem cell population rather than regenerating cilia.

The mucociliary epithelium of the *Xenopus* embryonic epidermis is similar in structure and function to the mammalian airway. The damage to cilia or MCCs in the mammalian airway is suggested to be repaired by replacing the damaged MCCs using basal stem cells[21,22]. Regeneration of cilia *per se* in mammalian airway MCCs has yet to be reported in the literature. Therefore, we investigated whether *Xenopus* MCCs regenerate cilia or rely on the stem cell-based replacement of damaged MCCs.

We performed live imaging of cilia regeneration to distinguish between the two hypotheses. We used *Xenopus* stem cell explants (animal caps) which auto-differentiate into an embryonic epidermis replete with MCCs. We harvested animal caps from *Xenopus* embryos injected with membrane RFP (to label cell and ciliary membrane) and grew them on fibronectin-coated slides. We deciliated the animal caps using the same protocol as the embryos and immediately began imaging MCCs using confocal microscopy. All MCCs showed a complete absence of cilia, indicating successful deciliation**.** Approximately 15 minutes post-deciliation, we could observe membrane RFP signal corresponding to regenerating cilia in MCCs. Our results demonstrate that *Xenopus* multiciliated epithelium regenerates cilia in the same MCCs and does not undergo stem cell-based renewal of damaged MCCs. **(Fig. S1A; Supplement Video 1)**.

Deciliation moderately affects the F-actin network but does not affect basal body number and polarity.

Next, we investigated whether the deciliation affects only the ciliary axoneme or cilia-associated structures, such as the apical F-actin network, basal body number, and polarity. Our results show that deciliation only moderately affected the apical F-actin network (calculated as the ratio of medial actin to cortical actin **(Fig. S1B)**. We used Chibby or Centrin to label basal bodies and Clamp to label rootlets to assess the effect of deciliation on basal body number, organization, and polarity [23]. Our results show that deciliation does not affect basal body number, organization, and polarity. **(Fig. S1C, D)**.

The TZ is removed by deciliation.

Next, we determined the location where the deciliation treatment severed cilia. Unicellular models such as *Chlamydomonas* and *Tetrahymena* lose cilia distal to the TZ and below the central pair (CP) microtubules[10,24–26]. Therefore, we hypothesized that *Xenopus* MCCs utilize a similar mechanism and would lose the ciliary axonemes distal to the TZ. To test the hypothesis, we labeled the TZ with an antibody to B9d1, a bona fide TZ protein[11,27–29]. To our surprise, B9d1 was lost from the deciliated MCCs **(Fig. 2A)**, suggesting that TZ was removed along with the ciliary axonemes. We did Transmission Electron Microscopy (TEM) to directly visualize the TZ in motile cilia to validate this unexpected result. TZ can be seen as an electron-dense H-shaped structure above the basal bodies [10,30–34]. In the deciliated embryos, we could see the basal bodies; however, the H-shaped structure corresponding to the TZ was lost entirely **(Fig. 2B)**. Taken together, these data demonstrate that, unlike unicellular organisms, deciliation in *Xenopus* MCCs removes the TZ with the ciliary axoneme.

While the TZ is lost with deciliation, the actual excision may happen at two distinct locations, distal to the basal body (between the basal body and TZ) and distal to the TZ (between TZ and CP), separately releasing the TZ and the axoneme into the medium[24,25,34]. Alternatively, deciliation may happen only distal to the basal bodies, in which case the TZ stays with the ciliary axoneme[10,24,32,34]. A previous proteomic study where authors deciliated *Xenopus* embryonic multiciliated skin found TZ proteins in their ciliary axoneme preparation suggested that the TZ is removed with the ciliary axonemes in *Xenopus* MCCs, supporting the later hypothesis [20]. To test the hypothesis that TZ was associated with the ciliary axoneme, we examined whether the B9d1 signal was associated with cilia post-deciliation. To that end, we performed an *in-situ* deciliation of embryos using deciliation buffer on poly-L-lysine coated coverslips. Once removed, cilia stick to the coverslip, stained for B9d1 and Ac. α-tubulin **(Fig. S2A).** Surprisingly, we did not see any B9d1 signal with cilia **(Fig. S2B)**. Notably, B9d1 is a soluble protein closely associated with the membrane-associated MKS protein complex in the TZ [9,27,35]. We examined ciliary axonemes with EM to examine if the detergent in the deciliation buffer is stripping the ciliary membrane and leading to the loss of the B9d1 signal. As expected, we could not observe any ciliary membrane (data not shown) supporting our hypothesis that loss of B9d1 is likely the result of loss of ciliary membrane. Therefore, to understand if the TZ remains associated with the axoneme after deciliation, we adopted an alternative approach of mechanical deciliation[36] **(Fig. S2A).** The advantage of this approach is that we did not use any detergent. We observed that cilia removed from the embryo consistently showed a B9d1 signal **(Fig. S2C)**. Thus, we demonstrate that the site of deciliation in *Xenopus* cilia is distal to the basal body, and the TZ remains attached to the ciliary axoneme.

TZ is dispensable for the initiation of ciliary axoneme assembly during regeneration.

Removal of the TZ during deciliation gave us a unique opportunity not afforded by any other vertebrate or invertebrate model to study the temporal relationship between TZ and axoneme assembly. The TZ is thought to form a molecular sieve-like barrier and serve as a "ciliary gate," regulating protein traffic into and out of the cilium[8,9]. Mutations in or knock-down/out of TZ proteins impair cilia assembly and function[11,27,29,32,37,38]. Further, recent studies have shown that Intraflagellar transport (IFT) trains assemble at the TZ, suggesting that TZ is essential for ciliary assembly and is predicted to precede ciliary axoneme assembly[10,14]. However, no direct evidence to support this hypothesis has been published.

Using our unique regeneration model, we directly tested this hypothesis. We examined the restoration of the B9d1 signal as a marker to track the reassembly of TZ during the first three hours of cilia regeneration. As expected, both the B9d1 and Ac. α-tubulin signals were completely lost after deciliation. One hour into regeneration, we were surprised to see the recovery of the Ac. α-tubulin but no detectable B9d1 signal. The B9d1 signal began to appear after 2 hours of

regeneration and further increased at 3 hours. **(Fig. 2A)**. We quantified the length of the recovered B9d1 signal in the MCCs. In control embryos (pre-deciliation), the length of the B9d1 signal was 1.33 μM (± 0..33, SEM); this signal increased from no signal at 1 hour to 0.55 μM (± 0.16, SEM) at 2 hours and 0.73 μM (±0.021, SEM) at 3 hours after deciliation (**Fig. 2C**) This result was unexpected because, contrary to the previous speculation, cells appeared to initiate ciliary axoneme assembly in the absence of a TZ.

We also used electron microscopy to directly analyze the early axoneme and TZ assembly steps during regeneration. Specifically, we performed the TEM on samples taken at 0, 20, and 90 minutes after deciliation (**Fig**. **2B**). At 20 minutes after deciliation, a small ciliary axoneme was present; however, the H-shaped structure indicating the presence of TZ was missing. The H-shaped structure of the TZ appeared 90 minutes after deciliation. The TEM data supported the results from our B9d1 immunofluorescence experiments. However, one of the limitations of the TEM approach is that the sections are very thin (~75nm), and we could easily miss the H-shaped structure when looking at a single section. To address this concern, we performed electron tomography of regenerating cilia at different time points (Pre., 0, 20 mins, 1 hr., 3 hrs., and 6 hrs.) to examine the timing of TZ assembly. Consistent with the TEM data, electron tomography results demonstrated that MCCs could initiate ciliary axoneme assembly without a TZ. The TZ was absent from the 20-minute tomogram and assembled between 1 and 3 hours after deciliation; by 6 hours, the TZ looked indistinguishable from controls **(Supplementary Videos 2-5)**. Our results suggest that the cells can incorporate TZ (or components of TZ) once the axoneme is assembled, suggesting a dynamic nature of TZ proteins. An earlier study in *Chlamydomonas* also reports the dynamic nature of a TZ protein, CEP290 incorporation into the pre-assembled axoneme[24]. During the mating process, there was an exchange of CEP290 from the wild-type cilia to the cilia of the CEP290 deficient mutant during the mating process [24]. While the previous study only showed one TZ protein CEP290 to be dynamically assembled in the cilia, we speculate that this could apply to many TZ proteins where they could be dynamically assembled or incorporated.

The CP assembles just distal to the TZ, but the role of the TZ, if any, in the positioning of the CP is still incompletely understood. Insight into this problem comes from *Chlamydomonas*, where a cell line with a mutation in the protein centrin (*vfl2* mutant) lacks the characteristic 'H' shaped TZ, and this results in CP assembly close to the basal body [39]. Since the initial assembly of the axoneme after deciliation occurs in the absence of a TZ, we investigated where the CP is assembled during the early stages of cilia regeneration. Reconstructed tomograms of regenerating cilium at 20 min post-deciliation indicated that the CP was assembled proximal to the basal body compared to the pre-deciliated (control) samples **(Fig. S3)**. This observation raises the question of how the CP position is subsequently adjusted to enable the construction of the TZ. Central pair nucleation and assembly in cilia have received little attention. A previous study suggests that proteins such as Katanin, WDR47, and CAMPSAP3 that localize distal to the basal bodies in MCCs play a critical role in initiating the assembly of the CP microtubules [40]. We speculate that, during regeneration, in the absence of TZ, these proteins can be activated following outer doublet assembly to build the CP. Subsequently, Katanin, a microtubule severing protein, could trim the CP MTs and create space to assemble the TZ. Another possibility is that the assembly of the TZ structure pushes up the CP. While this is speculation, our system allows us to understand the spatial and temporal relationship between assembling TZ and CP.

The structure of the ciliary axoneme is different at the proximal end, where the TZ is located, and the distal end, where the ciliary tip is located. Like the TZ, the ciliary tip comprises of a distinct protein complex of unknown function[6,7,31,41]. Some tip proteins are also localized to the CP microtubules[41]. Since the TZ showed a delayed regeneration, along with the displacement of CP, we asked if the ciliary tip was assembled after the ciliary shaft was built. To test this speculation, we used mScarlet-Sentan[42] and Clamp-GFP[57] proteins known to localize to the tip of motile cilia[42].

As reported earlier[42], we also observed that mScarlet-Sentan localized to ciliary tips in control Xenopus MCCs (**Fig. 3A**). Clamp-GFP was also present at the cilia rootlets (**Fig. S1**). After deciliation, ciliary Sentan and Clamp signals were lost as expected. However, when regeneration began, we noticed that small stubs of ciliary axonemes at 1 hr. post-deciliation were decorated entirely with the Sentan and Clamp signals. We could not show or quantify Clamp images because it is hard to distinguish the Clamp signal from the rootlets and small ciliary stubs. Therefore, we continued with assessing only the Sentan signal through the regeneration. At 2 and 3 hr. time points, we observed that the Sentan signal became stronger at the ciliary tips compared to the ciliary shaft. By 6 hours, the tip localization appeared like pre-deciliation controls. (**Fig. 3B**). Our data suggest that Ciliary tip proteins like Sentan and Clamp are trafficked immediately into regenerating cilia and gradually begin to concentrate at the tips.

TZ protein B9d1 is newly synthesized during cilia regeneration.

To explain the observation that assembly of the ciliary axoneme can occur in the absence of the TZ, we speculated that the TZ is a stable structure lacking protein turnover. Consequently, unlike proteins needed for axoneme assembly, e.g., tubulin and IFTs[16], the TZ proteins may not be present in the cytosolic pool (such as B9d1). Note we also do not observe any B9d1 signal at the bases of cilia or in the cytoplasm. Therefore, we hypothesized that cells might need to synthesize TZ proteins like B9d1 first to begin TZ assembly.

To test this hypothesis, we treated deciliated embryos with either vehicle (DMSO) alone or Cycloheximide (CHX), a protein synthesis inhibitor. We collected embryos every hour for the first 3 hours and quantified the B9d1 signal in the regenerating cilia. By 3 hours, control MCCs showed a significant increase in B9d1 signal. However, treatment with CHX completely abolished B9d1 recovery **(Fig. 4)**. These results suggest that B9d1, a TZ protein, is absent from the ciliary precursor pool. Though we tested this hypothesis only for a single TZ protein, B9d1, we hypothesize that other TZ proteins could also require transcription/translation at the time of deciliation, explaining the delay in TZ assembly during cilia regeneration.

One limitation of our results is that we have used only one protein, B9d1, to track the loss and reassembly of TZ. We attempted to localize multiple TZ proteins in *Xenopus,* but our attempts were unsuccessful as antibodies available to *Xenopus* are particularly limited. To overcome this shortcoming, we performed TEM and electron tomography to track the electron-dense region of the TZ. However, questions remain about the spatial and temporal sequence of other TZ proteins assembly during regeneration. Further, do all or only a few TZ proteins require new transcription/translation during regeneration? These question needs to be addressed by a specialized proteomic approach, such as proximity labeling with samples collected temporally, which will be addressed in future studies.

Synthesis of a new pool of ciliary proteins is required to support cilia regeneration.

Our results from the previous experiments raised an interesting question: do cilia regeneration in MCCs trigger new protein synthesis? From the live imaging experiments, we noted that cilia regeneration begins within approximately 15 minutes after deciliation. *Chlamydomonas* also begin cilia reassembly within minutes after deciliation. Studies have shown that *Chlamydomonas* uses the precursor pool of proteins to form rapid cilia reassembly; however, this precursor pool is insufficient to assemble full-length cilia [43,44]. Loss of cilia triggers the synthesis of new mRNA and proteins to support subsequent cilia assembly [44]. In contrast to *Chlamydomonas*, sea urchins contain excess proteins that can support full regeneration of cilia up to four times [45]. Therefore, we speculated that *Xenopus* MCCs might have a precursor pool of unassembled proteins that allow the cell to begin cilia reassembly quickly. However, whether *Xenopus* requires new transcription and translation of at least some proteins to complete cilia regeneration was not understood.

To test this hypothesis, we blocked protein synthesis immediately post-deciliation using Cycloheximide (CHX), forcing the cell to utilize the existing precursor pool in the cytoplasm. *Chlamydomonas* has only two cilia, but in *X. tropicalis* MCCs, there are ~150 cilia. Therefore, CHX treatment could result in either 1) regeneration of 150 wild-type-length cilia, 2) a full number of shorter cilia, or 3) a reduced number of cilia, either wild-type or perhaps longer than wild-type length. We observed that embryos treated with CHX showed a slower rate of cilia regeneration, as evidenced by consistently shorter cilia than controls during the entire regeneration period. **(Fig. 5 A-C)**. When we counted the number of cilia per MCC in CHX-treated embryos, we observed that CHX treatment led to significantly fewer cilia/cell compared to vehicle-treated controls. Interestingly, this reduction in number was gradual. Specifically, the number of regenerating cilia per MCC in CHX-treated embryos was highly variable at 1 hour ranging from 13-149 (cilia/MCC 64 ± 47.65; mean ± SD, **Fig. 5),** but the cilia number was dramatically decreased at 3 and then at 6 hours (3 hrs. 17.9 ± 9.82; 6 hrs. 9.89 ± 4.69, mean ± SD, **Fig. 5**) making fewer but about wild-type length cilia.

MCCs redistribute proteins among basal bodies to regenerate fewer but longer cilia.

We initially hypothesized that one of the contributing factors to the gradual decrease in the number of cilia from 1 to 6 hrs. in the CHX treatment could be a failure to maintain all basal bodies. Our data showed that embryos treated for 6 hours with CHX, either during normal development or regeneration, showed no difference in basal body number, suggesting that basal body loss was not contributing to reduction in cilia number **(Fig. 5E, Fig. S4).** Therefore, we hypothesized that MCCs somehow sense the absence of one or more rate-limiting proteins in the pool and respond by resorbing a subset of the regenerating cilia to support other cilia so fewer cilia can reach wild-type length. This phenomenon was observed previously in *Chlamydomonas*. When *Chlamydomonas* loses one of its two flagella, it resorbs the longer flagellum to redistribute the material to the regenerating cilium to support its assembly until both flagella reach the same length [16,43]. However, unlike *Chlamydomonas* cells, MCCs in *Xenopus* have hundreds of cilia; therefore, they may not use the same strategy.

IFT proteins are necessary to assemble the axoneme by transporting the axonemal proteins to the tip of the growing structure [19,46,47]. Ciliogenesis and cilia regeneration occurs by accumulating several ciliary proteins, including IFTs at the base of cilia in *Chlamydomonas* and *Xenopus* [10,16,19]. Therefore, we examined the pool of IFT43 at the base of regenerating cilia as a proxy for essential ciliogenesis proteins required for cilia regeneration in controls and CHX-treated embryos (Fig. 5A). In pre-deciliation and 0 hr. deciliated samples, all basal bodies were decorated with IFT43-GFP demonstrating that IFT43-GFP was similarly distributed among all basal bodies. In controls 1, 3, and 6 hrs. post-deciliation, all basal bodies remained equally decorated with IFT-43 GFP signal as expected. However, in the CHX-treated cells, IFT-43 gradually localized to only a subset of the basal bodies as regeneration progressed. We compared the number of basal bodies and the IFT43-GFP puncta associated with basal bodies to quantify this observation. We discovered that the number of basal bodies decorated with IFT-43 GFP signal gradually reduced from 1 hour (median Control 127 vs. 40 CHX treated) to 3 hours (median Control 129 to 16 in CHX treated) and then 6 hours (median Control 134 vs. 9 in CHX) (**Fig. 6 A and B**).

Next, we wanted to see if basal bodies decorated with IFT43-GFP regenerated cilia. We quantified the precursor pool enrichment (IFT43-GFP fluorescence intensity) around the basal bodies (Centrin-RFP) with and without cilia (Ac. α-tubulin) in the same cell for the CHX-treated samples. (**Fig. 6C**). Interestingly, there was a direct correlation between basal bodies decorated with IFT43-GFP and the presence of ciliary axoneme, suggesting that as MCCs sense the shortage of IFT43 protein and redistribute IFT43 between basal bodies to promote fewer but wild-type-length cilia (**Fig. 6A and C**). This is striking that MCCs possibly directly translocate proteins to create a subset

of basal bodies that can support ciliogenesis. We also noted that a few non-ciliated basal bodies have some IFT-43 GFP signal. This could be because IFT43-GFP was injected as mRNA, and the excess protein could be assembled at the basal bodies or translocated to a different basal body.

While *Chlamydomonas* also redistributes the proteins between cilia to coordinate their regeneration, significant differences between the model systems raise some fascinating questions about how cells sense information and make decisions that may require quantitative data [48,49] For example, *Chlamydomonas* has only two basal bodies that are proximally placed and physically connected. Thus, the basal bodies share the protein pool required for assembly. On the other hand, *Xenopus* MCCs nucleate hundreds of basal bodies. While they are connected via the cytoskeletal network [12,23,50], they are not physically connected like *Chlamydomonas*. Moreover, each cilium has its pool of proteins at the basal body to support its assembly. Given hundreds of basal bodies in *Xenopus* MCCs, how does inter-basal body transport operate? One possibility is that proteins are transported by diffusion to capture mechanism of protein transport from cytosol to cilia [19,51]. However, another possibility is the direct transport between basal bodies using a cytoskeleton (microtubule) network[52,53]. Hibbard et al. tested this possibility by depolymerizing microtubules with nocodazole and cold shock and showed that IFT recruitment at basal bodies could be independent of cortical microtubules [19]. However, this experiment was not carried out when the cell was experiencing a shortage of proteins, as is the case for CHX treatment. Our results also show that cells ensure that at least a few basal bodies can assemble wild-type length cilia raising questions about how these basal bodies are selected. One possibility is that ciliary axonemes must reach a minimum length to grow to wild-type length. This is not an issue in wild-type cells where proteins are abundant; however, in protein deficient state, only longer cilia that reached the minimum length continue assembling, whereas others resorb because of competition for the available pool of proteins.

In conclusion, our study reveals new and significant findings and raises exciting questions about the mechanisms of cilia regeneration in vertebrate MCCs. We show that the location for severing the ciliary axoneme in MCCs was distal to the basal body, which differs from unicellular organisms like *Chlamydomonas*. Most interestingly, MCCs initiate the assembly of the ciliary tip and ciliary shaft before the assembly of the TZ, after which both grow concurrently. One possibility is that there is a lack of a cytosolic pool for one or more proteins that are rate-limiting for TZ assembly. These findings raise intriguing questions about the spatial-temporal sequence of cilia assembly and the importance of TZ in ciliary assembly. For example, is the TZ dispensable for motile ciliogenesis? When are other components needed for ciliary stability (e.g., microtubule inner proteins) transported into the cilium? How do MCCs decide the spatial location of the central pair microtubules in the absence of TZ? Moreover, the study also highlights the importance of new transcription/translation in completing cilia regeneration. Without protein synthesis during cilia regeneration, MCCs produce few but about wild-type length cilia. The study provides insights into the cellular decision-making process that regulates the size and number of organelles, such as cilia, when cells are damaged and have limited resources available for repair.

MATERIALS AND METHODS

Animal husbandry and *in-vitro* fertilization

Frogs (*Xenopus tropicalis*) were bred and housed in a vivarium using protocols approved by the University of Virginia Institutional animal care and use committee (IACUC). Embryos needed for experiments were generated using *in-vitro* fertilization as described before [23,54]. Briefly, the testes from male frogs were crushed in 1x MBS (pH-7.4) with 0.2% BSA and added to eggs obtained from the female frogs. After 3 minutes of incubation, freshly made 0.1x MBS (pH-7.8) was added, and the eggs were incubated for ten more minutes till contraction of the animal pole of the eggs

was visible. The jelly coat was removed using 3% cysteine in 1/9 x MR solution (pH 7.8-8.0) for 6 minutes. The embryos were either microinjected with DNA/RNA and raised at 25°C or 28°C till they reached appropriate stages for fixation and staining or mucociliary organoid (animal cap) dissection. Embryos were staged as described previously [55].

Animal cap / mucociliary organoid dissection

Embryos at stage 10 were used for animal cap dissection. The animal pole from the stage 10 embryos was dissected using a fine hair tool in a pool of Danilchik's for Amy (DFA) medium. The dissected tissue was trimmed to remove the equatorial cells from the sides. This tissue was then laid on a coverslip or glass slide coated with fibronectin (Sigma Cat No. F1141) immersed in DFA solution. The tissue was allowed to grow and spread on the fibronectin-coated slides/coverslips overnight till they reached stage 28.

DNA, RNA, and microinjections

Plasmids used in this study are listed in the key resource table. For generating Chibby-BFP, the full-length Chibby gene was cloned to the N-terminus of mtagBFP2 in the pCS2+ vector using Gibson assembly. RNA used in this study was generated by linearizing the plasmids and *in-vitro* transcribed using the mMessage and mMachine SP6 transcription kit (Thermo Fisher Scientific). Microinjections were done using glass needles using the Pico-liter microinjection system (Warner instruments). All the microinjections were done at the 1-cell stage except for Figure 2, where the membrane RFP was injected in 1 of the four blastomeres at the four-cell stage.

Chemical deciliation of embryos and mucociliary organoids

Embryos, after they reach stage 28, were used for deciliation experiments. A basket was designed for deciliation by cutting a 50 ml centrifuge tube. One of the open ends of the tube was heat-sealed with a muslin cloth. A 6-well plate was filled with deciliation solution (75 mM $CaCl_2$, 0.02% NP40 in 1/3 MR solution). The rest of the five wells were filled with 1/9x MR. Anesthetized embryos were transferred to this container and dipped in a deciliation solution (75 mM $CaCl_2$, 0.02% NP40 alternative in 1/3 MR solution) in a 6-well plate for 10-15 seconds. Post-deciliation, embryos with the container were dipped/washed with 1/9x MR in the rest of the wells of the 6-well plate. The embryos were then transferred to a petri dish with 1/9x MR with gentamicin and incubated at 28°C. Embryos were collected during various stages of cilia regeneration, as mentioned in the text and figure legends. For animal caps, the glass slide/coverslip was removed from the DFA medium and dipped in the deciliation solution for 15 seconds. Post-deciliation, the glass side/coverslip was dipped in 1/9x MR for 30 seconds and transferred to DFA until they regenerated cilia to the appropriate stage. Control or deciliated embryos were transferred to 1/9 X MR solution containing 10 mg/ml of cycloheximide (CHX) or DMSO for cycloheximide experiments.

Immunofluorescence staining and imaging.

The *X. tropicalis* embryos used for the study were fixed post-stage 28 with appropriate fixative agents. For most experiments, 4% paraformaldehyde (PFA) was used as a fixative, and 100% chilled methanol was used to fix the embryos for anti-B9d1 staining. After fixation, the embryos were washed three times with PBST (1x PBS with 0.2% Triton X-100) for 10 mins each and then incubated in a blocking solution (3% BSA in PBST) for 1 hour. Appropriate antibody was added to the embryos, incubated for 1 hour at room temperature, and rewashed three times for 10 mins each with PBST. A conjugated secondary antibody was used to stain embryos for 1 hour. The embryos were washed three times with PBST, stained with phalloidin in PBST for 45 minutes, and washed once post-staining, and the embryos were mounted and imaged. Confocal imaging was performed using the Leica DMi8 SP8 microscope using a 40x oil immersion objective (1.3 NA). Images were captured at 1x or 4x zoom and adjusted (brightness and contrast), analyzed, cropped in Fiji, and assembled in Adobe Illustrator software.

Sample preparation for electron tomography

Xenopus stage 26-28 embryos Pre and post deciliation were fixed in 2.5% glutaraldehyde and 2% paraformaldehyde in 0.1M sodium cacodylate buffer pH-7.4 for 1 hour, rinsed in the buffer, then post-fixed in 1% osmium tetroxide. Subsequently, embryos were rinsed in buffer and stained in 2% aqueous uranyl acetate for another hour. Embryos were rinsed and dehydrated in an ethanol series (15min 30% ethanol, 15min 50% ethanol, 15min 70% ethanol, 15min 90% ethanol, 3x 30min 100% ethanol). Dehydrated embryos were infiltrated with EPON Araldite (Electron Microscopy Sciences) and polymerized overnight at 60 C. Serial semi-thick sections (200 nm) were cut using an Ultracut UCT Microtome (Leica Microsystems, Vienna, Austria). Sections were collected on piliform-coated copper slot grids and poststained with 2% uranyl acetate in 70% methanol, followed by Reynold's lead citrate57.

Data acquisition by electron tomography.

Colloidal gold particles (15 nm; Sigma-Aldrich) were attached to both sides of semi-thick sections collected on copper slot grids to serve as fiducial markers for subsequent image alignment. For dual-axis electron tomography, a series of tilted views were recorded using a TECNAI F20 transmission electron microscope (FEI Company, Eindhoven, The Netherlands) operated at 200 kV. Images (4K x 4K) were captured every 1h over a ±60 range and a pixel size of 2.3nm using a TVIPS CCD camera. We used the IMOD software package (http://bio3d.colourado.edu/imod) for image processing, which contains all the programs needed for calculating electron tomograms. The tilted views were aligned using the positions of the colloidal gold particles as fiducial markers. Tomograms were computed for each tilt axis using the R-weighted back-projection algorithm. Reconstructed tomograms were flattened.

Image analysis, quantification, and statistics

All the experiments were repeated three times. All the measurements and analyses were performed on at least three embryos. Sample size, indicated by "n" values, are included in the figure legends. For length measurement (cilia length and TZ length), at least three cells per embryo were chosen randomly; however, it was ensured that only those cilia/signals which were distinct and not overlapping (or tangled) with neighboring ones were measured. For statistical analysis, Prism ver. 9.2 was used. The type of analysis and p values and the significance are included in the figure legends. The F-actin intensity measurements were done using Fiji. The cortical actin refers to the actin network along the MCC boundary, while the medial actin refers to the F-actin network at the apical surface of the MCC. The intensity measurements were performed using a line or polygon tool in Fiji, as described in an earlier study[12]. The normalization of F-actin is the ratio of intensities of median F-actin to cortical F-actin. For orientation calculations, images were taken after aligning the embryos horizontally from anterior on the left to posterior on the right and stained for Clamp-GFP (rootlet) and Centrin-RFP (basal body). The Clamp-GFP orientations were calculated in MATLAB R2021a using image processing and circular statistics toolboxes. The cilia orientations were drawn by hand from rootlet to basal body using the 'drawline' command. The angles were calculated with respect to the global X-axis in the cartesian coordinate system (first point starting at 0,0) using the command 'atan2d', which gives the angles from 0° to $+180^o$ in a counterclockwise direction (quadrants I and II) and 0° to -180° in a clockwise direction (Quadrants IV and III). 26 and 21 multiciliated cells were analyzed for control and deciliated embryos, respectively, with an average of 112 cilia orientations (~60-200 cilia per cell) in each cell for each condition. For IFT43-GFP and Centrin RFP calculation, a total number of Centrin-RFP dots were calculated in each MCC, and the corresponding IFT43-GFP surrounding the Centrin-RFP signal was also calculated. For the IFT43-GFP fluorescence intensity calculations, a circular ROI between 0.646-0.680 μm^2 was drawn around ciliated and non-ciliated Centrin-RFP puncta. The mean gray value of the IFT43-GFP channel was calculated, and the values were

normalized from 0-1. Each dataset had a mean gray value from 5 ciliated and five non-ciliated basal bodies, and normalization was done using the following formula:

Normalized value = (Mean gray value – Min value in the data set) / (Max value in the dataset- Min value in the data set)

Key resource table

Antibodies			
Name	**Marker**	**Make and Cat. No.**	**Remark**
Mouse Anti-Acetylated α-tubulin (6-11B1)	Ciliary axoneme	Sigma	PFA fix, 1:1000
Rabbit mAb Acetyl-α-Tubulin (Lys40) (D20G3)	Ciliary axoneme	Cell Signalling technology (#5335)	Methanol Fix, 1: 500
Rabbit mAb Acetyl-α-Tubulin (Lys40) (D20G3) (Alexa Fluor® 647 Conjugate)	Ciliary axoneme	Cell Signaling Technology (#81502)	PFA fix, 1: 25
Mouse pAb Anti-B9d1	Transition Zone	Sigma (SAB1409114)	Methanol Fix, 1:50
Chicken anti Mouse conjugated to Alexa fluor 488	NA	Invitrogen	1:500
Anti-Rabbit conjugated to Alexa fluor 647	NA	Jackson	1:500
Phalloidin conjugated to Alexa fluor 488	Actin	Invitrogen	1:50
Phalloidin conjugated to Alexa fluor 647	Actin	Invitrogen	1:50
DNA/RNA			
Name	**Marker**	**Conc. injected**	**Source**
Chibby-tagBFP2	Basal body	100 pg (RNA)	This study
mScarlet-Sentan	Cilia tip	200 pg(RNA)	This study
GFP-Clamp	Rootlets	200 pg (RNA)	[56]
Centrin-RFP	Basal body	100 pg (RNA)	[56]
MemRFP	Cell and Ciliary membrane	100 pg(RNA)	[57]
IFT43-GFP	Cilia base/Cilia	150pg (RNA)	[19]

ACKNOWLEDGMENTS

The authors would like to express their gratitude to Dr. Bob Bloodgood and the members of the Kulkarni Lab for their invaluable feedback and thorough review of this manuscript. Appreciation is also extended to Dr. Mustafa Khokha for initial discussions and the intellectual guidance for the project. Acknowledgment is also due to the Molecular Electron Microscopy Core and the Advanced Microscopy Facility at UVA. Lastly, we are grateful for the NIH Pathway to Independence, K99/R00 (K99HL133606 and R00HL133606) grant which was awarded to Saurabh Kulkarni.

FIGURE LEGENDS

Figure 1: Deciliation and regeneration of cilia from the mucociliary epithelium of *Xenopus tropicalis*.

A) Cartoon depiction of the deciliation and regeneration protocol of *X. tropicalis* embryos.

B) Pre-deciliated embryos (Pre.) and embryos during the regeneration (0 hr.,1 hr., 3 hr., 6 hr.) stained for cilia (Ac. α-tubulin in magenta) and F-actin (phalloidin in green) are depicted. For each time point, the top panel shows the entire embryo, the lower left panel is a zoomed image of the multiciliated epithelium, and the lower right panel is an SEM image of the embryonic epithelium. Black arrows in the SEM image point to MCCs.

C) Graph depicts cilia length pre- and post-deciliation. The values in parenthesis indicate the number of cilia measured from three trials (**** - $p<0.0001$, *** - $p<0.001$, ns - not significant, ANOVA analysis was followed by Tukey's multiple comparison test).

Figure 2: Loss and regeneration of transition zone

A) MCCs labeled with B9d1 antibody (TZ, green) and Ac. α-tubulin (cilia, magenta) in embryos pre-, 0 hr., and during cilia regeneration. While dotted lines depict MCC shape.

B) Representative TEM images of cilia pre-, 0 hr., and during the regeneration (0 mins, 20 mins, and 90 mins). The TZ can be seen as an 'H' shaped structure between the axoneme and basal body (indicated by a black arrowhead). Post-deciliation samples show a complete the loss of TZ. TZ is absent after 20 mins of cilia regeneration. A faint electron-dense TZ structure can be seen after 90 mins of cilia regeneration.

C) Length of the B9d1 signal was measured pre- and during cilia regeneration (at 2 hr. and 3 hr.) The B9d1 signal was absent at earlier time points (0 hr. and 1 hr.). The values in parenthesis indicate the number of cilia measured from three trials (**** - $p<0.0001$; ns - not significant, One-way ANOVA analysis followed by Tukey's multiple comparison test).

Figure 3: Ciliary tip protein Sentan is localized to the ciliary axoneme during the early stages of regeneration.

A) MCCs labeled with mScarlet-Sentan (ciliary tip, magenta), and Ac. α-tubulin (cilia, green) at various stages of cilia regeneration. Sentan can be seen at the tips of cilia in pre-deciliated samples. After 1 hr. post-deciliation, Sentan can be seen in the cilia. At 2 hrs., Sentan can be seen concentrating at the ciliary tips. While at 3 and 6 hr., Sentan signal appears more like pre-deciliated samples.

B) The Sentan signal length (left panel) and cilia length (right panel) were measured and compared among different timepoints. The values in parenthesis indicate the number of cilia measured from three trials. (**** - $p<0.0001$; ns - not significant, Kruskal-Wallis test, followed by Dunn's test).

Figure 4: TZ protein B9d1 requires new protein synthesis during regeneration.

A) Embryos treated with DMSO alone (Vehicle) or cycloheximide (CHX) in DMSO were stained for B9d1 (a TZ protein) and Ac. α-tubulin (cilia) and collected pre-deciliation and during cilia regeneration (0 hr., 1hr., 2 hr., 3 hr.). The cell outline is marked in the green (B9d1) channel, and the dashed square box in the B9d1 channel is zoomed and depicted in the inset. While cilia can regenerate in both treatments (controls and CHX), the B9D1 signal is recovered only in controls and remains completely absent in the CHX-treated samples at 2hr. And 3 hr. timepoints. Ax: Axoneme, TZ: transition zone, BB: Basal body

B) The percent of MCCs positive for the B9d1 signal are shown in green, and absent B9d1 signal are shown in magenta. Numbers in parentheses indicate the number of MCCs counted. A between the samples (***- $p>0.001$, chi-square test using VassarStats to test the significance)

Figure 5: Complete cilia regeneration requires new protein synthesis.
A) Embryos treated with DMSO (Vehicle) and cycloheximide (CHX) in DMSO were stained for F-actin (green) and Ac. α-tubulin (cilia) and collected pre-deciliation, 0 hr., and during cilia regeneration (0 hr., 1hr., 3 hr.,6 hr.)
B) Cartoon depiction of results showing the effect of CHX on cilia regeneration.
C) Quantification of cilia length (mean ± SEM) during regeneration in the vehicle and CHX-treated groups. For all samples, 28 cilia were measured except at 5 and 6 hrs., where 27 cilia were measured.
D) Graph showing the effect of CHX treatment on cilia number per MCC during regeneration. The number of cilia in each MCC from CHX-treated samples was counted. The number in parenthesis indicates the number of MCCs counted. (**** - p>0.0001, Kruskal Wallis test, followed by Dunn's multiple comparison test)
E) Graph shows the comparison of basal body number in MCCs under all the treatment conditions. The number in parenthesis indicates the number of MCCs counted from three trials. (ns = not significant. Kruskal Wallis test, followed by Dunn's multiple comparison test).

Figure 6: Distribution of ciliary precursor IFT43 pool in MCCs.
A) Stage 28 embryos injected with IFT43-GFP (green) and Centrin-RFP (red hot) were deciliated (0 hr.) and were split into two batches (DMSO and CHX) and allowed to regenerate cilia for 6 hours. After fixation, the embryos were stained for cilia(magenta). Note that the control MCCs at all time points (1 hr., 3hr., and 6hr.) have multiple cilia regenerating, and the IFT43-GFP intensity is similar at every basal body (marked with Centrin-RFP). In contrast, the number of cilia is reduced later in CHX-treated samples, and the IFT43-GFP is enriched at the ciliated basal bodies.
B) Number of basal bodies that show positive IFT43-GFP signal. Note that in all control samples (1 hr., 3hr., and 6hr.), all basal bodies were occupied by IFT43-GFP puncta. In contrast, the CHX-treated samples showed a gradual reduction in the basal bodies occupied by IFT43-GFP from 1 to 6 hrs. The number in parenthesis indicates the number of MCCs counted. (**** - p<0.0001, *** - p=0.001, Two-tailed t-test.)
C) The intensity of IFT-43-GFP associated with ciliated vs. non-ciliated basal bodies in the same MCC (in CHX-treated samples). A total of 10 basal bodies per cell (5 ciliated and five non-ciliated) were chosen, and the mean gray value was estimated and normalized to the maximum and the minimum value in the set. The number in parenthesis indicates the number of basal bodies (with and without IFT43-GFP) analyzed. (**** - p<0.0001, Two-tailed t-test)

Figure 7: Model for cilia regeneration in *Xenopus tropicalis* embryos
Cilia regeneration in *Xenopus tropicalis* embryonic MCCs is multi-staged and is depicted in the cartoon. Post-deciliation, the TZ is lost with cilia. During stage 1 of regeneration (0-2 hours), the cilia grow without the TZ. Also, the cilia tip proteins Sentan and Clamp are immediately trafficked into ciliary axoneme, and CP is assembled closer the basal body. By stage 2 (2-4 hours), partial transition zone appears, ciliary tip proteins begin to accumulate at the distal end of the axoneme. The cilia look similar to pre-deciliated samples by the end of regeneration.

SUPPLEMENTARY FIGURE LEGENDS

Figure S1: Deciliation affects apical F-actin, but the basal body number is unaffected.
A) Montage of regenerating cilia (mem-RFP) in the animal caps. The mem-RFP signal specks can be seen emerging from the cell's surface by ~12 mins, eventually growing into beating cilia (see Supplement video 1).
B) Pre- and post-deciliation MCCs are depicted that are stained for cilia(magenta) and F-actin(green). The normalized F-actin intensity significantly differs in Pre and 0-hr. deciliated samples. Normalized F-actin intensity is the ratio of medial actin to cortical actin (see methods

section for description). (**** - p<0.0001 Mann-Whitney test). The values in parenthesis indicate the number of MCCs measured from three trials.
C) Number of basal bodies labeled with Chibby-GFP (cyan) is not affected after deciliation. The values in parenthesis indicate the number of MCCs measured from three trials. (ns = not significant, Mann-Whitney test.
D) Deciliation does not affect basal body polarity. Basal body polarity was determined by measuring the orientation of rootlets labeled with Clamp-GFP (green) with their respective basal body labeled with Centrin-RFP (magenta) and represented in the rose plot.

Figure S2: Transition zone is removed with cilia upon deciliation.
A) Schematic of the chemical and mechanical deciliation methods.
B, C) Cilia with chemical deciliation lose the B9d1 signal, possibly due to the loss of membrane with detergent in the deciliation buffer, whereas the B9d1 signal is maintained with mechanical deciliation.

Figure S3: Montage from cilia tomogram depicting the central pair assembly close to the basal body.
A and A') Montage of the ciliary axoneme from a control MCC. The central pair (magenta dotted line) assembles distant from the cell body (distance shown with black lines).
B and B') Montage of the regenerating cilia 20 minute post-deciliation. The TZ is absent, and the central pair (magenta dotted line) assembles closer to the cell body than controls (distance shown with black lines).

Figure S4: Blocking new protein synthesis does not affect basal body number in a steady state or during regeneration.
A) Stage 28 embryos injected with Chibby-BFP (green) were transferred to DMSO containing 1/9 MR (vehicle) or 1/9 MR containing cycloheximide (CHX) during development for 3 and 6 hours. Embryos were fixed and stained for cilia using acetylated α-tubulin.
B) After deciliation, the embryos were transferred to DMSO (vehicle) or 1/9 MR containing CHX, and cilia were allowed to regenerate for 3 and 6 hours. Embryos were fixed and stained for cilia using acetylated α-tubulin. The Chibby puncta were counted in all samples (deciliation and regeneration), and the basal body number quantification is shown in graph Fig. 4E.

SUPPLEMENTARY VIDEO LEGENDS

Supplement Video 1: Mucociliary epithelium regenerates cilia in the same MCC.
Live imaging of animal caps dissected from embryos injected with membrane-RFP RNA. Imaging was started approximately 2 minutes post-deciliation. The time stamp on the video is when the imaging was started and not the time of deciliation.

Supplement video 2 - 6: Cilia regeneration tomogram data.
Tomograms from control and regenerating MCCs. Cilium from the control sample shows the presence of TZ, indicated by an 'H' shaped electron-dense structure (video 2). Note that this structure is missing in samples after 20 minutes of cilia regeneration (video 3) and begins to appear after 1 hour (video 4). By the end of 3 hours (video 5) and 6 hours (video 6) of cilia regeneration, the tomograms reveal complete regeneration of the transition zone.

REFERENCES

1. Klena, N.T., Gibbs, B.C., and Lo, C.W. (2017). Cilia and Ciliopathies in Congenital Heart Disease. Cold Spring Harb Perspect Biol 9. 10.1101/cshperspect.a028266.

2. Noone, P.G., Leigh, M.W., Sannuti, A., Minnix, S.L., Carson, J.L., Hazucha, M., Zariwala, M.A., and Knowles, M.R. (2004). Primary Ciliary Dyskinesia. Am J Respir Crit Care Med *169*, 459–467. 10.1164/rccm.200303-365OC.
3. Afzelius, B.A. (2004). Cilia-related diseases. J Pathol *204*, 470–477. https://doi.org/10.1002/path.1652.
4. Ishikawa, T., Ueno, H., Omori, T., and Kikuchi, K. (2021). Cilia and centrosomes: Ultrastructural and mechanical perspectives. Semin Cell Dev Biol *110*, 61–69. https://doi.org/10.1016/j.semcdb.2020.03.007.
5. Nicastro, D., Schwartz, C., Pierson, J., Gaudette, R., Porter, M.E., and McIntosh, J.R. (2006). The Molecular Architecture of Axonemes Revealed by Cryoelectron Tomography. Science (1979) *313*, 944–948. 10.1126/science.1128618.
6. Reynolds, M.J., Phetruen, T., Fisher, R.L., Chen, K., Pentecost, B.T., Gomez, G., Ounjai, P., and Sui, H. (2018). The Developmental Process of the Growing Motile Ciliary Tip Region. Sci Rep *8*, 7977. 10.1038/s41598-018-26111-2.
7. Legal, T., Tong, M., Black, C., Valente Paterno, M., Gaertig, J., and Bui, K.H. (2023). Molecular architecture of the ciliary tip revealed by cryo-electron tomography. bioRxiv. 10.1101/2023.01.03.522627.
8. Kee, H.L., Dishinger, J.F., Lynne Blasius, T., Liu, C.J., Margolis, B., and Verhey, K.J. (2012). A size-exclusion permeability barrier and nucleoporins characterize a ciliary pore complex that regulates transport into cilia. Nat Cell Biol *14*, 431–437. 10.1038/ncb2450.
9. Okazaki, M., Kobayashi, T., Chiba, S., Takei, R., Liang, L., Nakayama, K., and Katoh, Y. (2020). Formation of the B9-domain protein complex MKS1–B9D2–B9D1 is essential as a diffusion barrier for ciliary membrane proteins. Mol Biol Cell *31*, 2259–2268. 10.1091/mbc.E20-03-0208.
10. van den Hoek, H., Klena, N., Jordan, M.A., Alvarez Viar, G., Righetto, R.D., Schaffer, M., Erdmann, P.S., Wan, W., Geimer, S., Plitzko, J.M., et al. (2022). In situ architecture of the ciliary base reveals the stepwise assembly of intraflagellar transport trains. Science (1979) *377*, 543–548. 10.1126/science.abm6704.
11. Li, C., Jensen, V.L., Park, K., Kennedy, J., Garcia-Gonzalo, F.R., Romani, M., De Mori, R., Bruel, A.L., Gaillard, D., Doray, B., et al. (2016). MKS5 and CEP290 Dependent Assembly Pathway of the Ciliary Transition Zone. PLoS Biol *14*, 1–29. 10.1371/journal.pbio.1002416.
12. Kulkarni, S.S., Griffin, J.N., Date, P.P., Liem, K.F., and Khokha, M.K. (2018). WDR5 Stabilizes Actin Architecture to Promote Multiciliated Cell Formation. Dev Cell *46*, 595-610.e3. https://doi.org/10.1016/j.devcel.2018.08.009.
13. Gakovic, M., Shu, X., Kasioulis, I., Carpanini, S., Moraga, I., and Wright, A.F. (2011). The role of RPGR in cilia formation and actin stability. Hum Mol Genet *20*, 4840–4850. 10.1093/hmg/ddr423.
14. Molla-Herman, A., Ghossoub, R., Blisnick, T., Meunier, A., Serres, C., Silbermann, F., Emmerson, C., Romeo, K., Bourdoncle, P., Schmitt, A., et al. (2010). The ciliary pocket: an endocytic membrane domain at the base of primary and motile cilia. J Cell Sci *123*, 1785–1795. 10.1242/jcs.059519.
15. Rannestad, J. (1974). THE REGENERATION OF CILIA IN PARTIALLY DECILIATED TETRAHYMENA. J Cell Biol *63*, 1009–1017.
16. Craft, J.M., Harris, J.A., Hyman, S., Kner, P., and Lechtreck, K.F. (2015). Tubulin transport by IFT is upregulated during ciliary growth by a cilium-autonomous mechanism. Journal of Cell Biology *208*, 223–237. 10.1083/jcb.201409036.

17. Silflow, C.D., and Lefebvre, P.A. (2001). Assembly and Motility of Eukaryotic Cilia and Flagella. Lessons from Chlamydomonas reinhardtii . Plant Physiol *127*, 1500–1507. 10.1104/pp.010807.
18. Werner, M.E., and Mitchell, B.J. (2013). Chapter Ten - Using Xenopus Skin to Study Cilia Development and Function. In Cilia, Part B, W. F. B. T.-M. in E. Marshall, ed. (Academic Press), pp. 191–217. https://doi.org/10.1016/B978-0-12-397944-5.00010-9.
19. Hibbard, J.V.K., Vazquez, N., Satija, R., and Wallingford, J.B. (2021). Protein turnover dynamics suggest a diffusion-to-capture mechanism for peri-basal body recruitment and retention of intraflagellar transport proteins. Mol Biol Cell *32*, 1171–1180. 10.1091/mbc.E20-11-0717.
20. Sim, H.J., Yun, S., Kim, H.E., Kwon, K.Y., Kim, G.H., Yun, S., Kim, B.G., Myung, K., Park, T.J., and Kwon, T. (2020). Simple Method to Characterize the Ciliary Proteome of Multiciliated Cells. J Proteome Res *19*, 391–400. 10.1021/acs.jproteome.9b00589.
21. Tadokoro, T., Wang, Y., Barak, L.S., Bai, Y., Randell, S.H., and Hogan, B.L.M. (2014). IL-6/STAT3 promotes regeneration of airway ciliated cells from basal stem cells. Proceedings of the National Academy of Sciences *111*, E3641–E3649. 10.1073/pnas.1409781111.
22. Parekh, K.R., Nawroth, J., Pai, A., Busch, S.M., Senger, C.N., and Ryan, A.L. (2020). Stem cells and lung regeneration. American Journal of Physiology-Cell Physiology *319*, C675–C693. 10.1152/ajpcell.00036.2020.
23. Kulkarni, S., Marquez, J., Date, P., Ventrella, R., Mitchell, B.J., and Khokha, M.K. (2021). Mechanical stretch scales centriole number to apical area via Piezo1 in multiciliated cells. Elife *10*, e66076. 10.7554/eLife.66076.
24. Craige, B., Tsao, C.C., Diener, D.R., Hou, Y., Lechtreck, K.F., Rosenbaum, J.L., and Witman, G.B. (2010). CEP290 tethers flagellar transition zone microtubules to the membrane and regulates flagellar protein content. Journal of Cell Biology *190*, 927–940. 10.1083/jcb.201006105.
25. Parker, J.D.K., Hilton, L.K., Diener, D.R., Rasi, M.Q., Mahjoub, M.R., Rosenbaum, J.L., and Quarmby, L.M. (2010). Centrioles are freed from cilia by severing prior to mitosis. Cytoskeleton *67*, 425–430. 10.1002/cm.20454.
26. Dean, S., Moreira-Leite, F., Varga, V., and Gull, K. (2016). Cilium transition zone proteome reveals compartmentalization and differential dynamics of ciliopathy complexes. Proceedings of the National Academy of Sciences *113*, E5135–E5143. 10.1073/pnas.1604258113.
27. Chih, B., Liu, P., Chinn, Y., Chalouni, C., Komuves, L.G., Hass, P.E., Sandoval, W., and Peterson, A.S. (2012). A ciliopathy complex at the transition zone protects the cilia as a privileged membrane domain. Nat Cell Biol *14*, 61–72. 10.1038/ncb2410.
28. Tony Yang, T., Su, J., Wang, W.J., Craige, B., Witman, G.B., Bryan Tsou, M.F., and Liao, J.C. (2015). Superresolution pattern recognition reveals the architectural map of the ciliary transition zone. Sci Rep *5*, 1–13. 10.1038/srep14096.
29. Garcia-Gonzalo, F.R., Corbit, K.C., Sirerol-Piquer, M.S., Ramaswami, G., Otto, E.A., Noriega, T.R., Seol, A.D., Robinson, J.F., Bennett, C.L., Josifova, D.J., et al. (2011). A transition zone complex regulates mammalian ciliogenesis and ciliary membrane composition. Nat Genet *43*, 776–784. 10.1038/ng.891.
30. Ringo, D.L. (1967). STRUCTURE APPARATUS MOTION OF THE AND IN CHLAMYDOMONAS Light Microscopy. J Cell Biol, 543–571.

31. Portman, R.W., LeCluyse, E.L., and Dentler, W.L. (1987). Development of microtubule capping structures in ciliated epithelial cells. J Cell Sci *87*, 85–94. 10.1242/jcs.87.1.85.
32. Awata, J., Takada, S., Standley, C., Lechtreck, K.F., Bellvé, K.D., Pazour, G.J., Fogarty, K.E., and Witman, G.B. (2014). NPHP4 controls ciliary trafficking of membrane proteins and large soluble proteins at the transition zone. J Cell Sci *127*, 4714–4727. 10.1242/jcs.155275.
33. Greenan, G.A., Vale, R.D., and Agard, D.A. (2020). Electron cryotomography of intact motile cilia defines the basal body to axoneme transition. Journal of Cell Biology *219*. 10.1083/jcb.201907060.
34. Diener, D.R., Lupetti, P., and Rosenbaum, J.L. (2015). Proteomic Analysis of Isolated Ciliary Transition Zones Reveals the Presence of ESCRT Proteins. Current Biology *25*, 379–384. https://doi.org/10.1016/j.cub.2014.11.066.
35. Garcia-gonzalo, F.R., Corbit, K.C., Sirerol-piquer, M.S., Otto, E.A., Noriega, T.R., Seol, A.D., Robinson, J.F., Bennett, C.L., Josifova, D.J., García-verdugo, J.M., et al. (2012). HHS Public Access. *43*, 776–784. 10.1038/ng.891.A.
36. Kiesel, P., Alvarez Viar, G., Tsoy, N., Maraspini, R., Gorilak, P., Varga, V., Honigmann, A., and Pigino, G. (2020). The molecular structure of mammalian primary cilia revealed by cryo-electron tomography. Nat Struct Mol Biol *27*, 1115–1124. 10.1038/s41594-020-0507-4.
37. Wang, L., Wen, X., Wang, Z., Lin, Z., Li, C., Zhou, H., Yu, H., Li, Y., Cheng, Y., Chen, Y., et al. (2022). Ciliary transition zone proteins coordinate ciliary protein composition and ectosome shedding. Nat Commun *13*, 3997. 10.1038/s41467-022-31751-0.
38. Craige, B., Tsao, C.-C., Diener, D.R., Hou, Y., Lechtreck, K.-F., Rosenbaum, J.L., and Witman, G.B. (2010). CEP290 tethers flagellar transition zone microtubules to the membrane and regulates flagellar protein content. Journal of Cell Biology *190*, 927–940. 10.1083/jcb.201006105.
39. Sanders, M.A., and Salisbury, J.L. (1994). Centrin plays an essential role in microtubule severing during flagellar excision in Chlamydomonas reinhardtii. Journal of Cell Biology *124*, 795–805. 10.1083/jcb.124.5.795.
40. Liu, H., Zheng, J., Zhu, L., Xie, L., Chen, Y., Zhang, Y., Zhang, W., Yin, Y., Peng, C., Zhou, J., et al. (2021). Wdr47, Camsaps, and Katanin cooperate to generate ciliary central microtubules. Nat Commun *12*, 5796. 10.1038/s41467-021-26058-5.
41. Dentler, W.L. (1984). Attachment of the cap to the central microtubules of Tetrahymena cilia. J Cell Sci *66*, 167–173. 10.1242/jcs.66.1.167.
42. Kubo, A., Yuba-Kubo, A., Tsukita, S., Tsukita, S., and Amagai, M. (2008). Sentan: a novel specific component of the apical structure of vertebrate motile cilia. Mol Biol Cell *19*, 5338–5346. 10.1091/mbc.e08-07-0691.
43. Rosenbaum, J.L., and Child, F.M. (1967). Flagellar regeneration in protozoan flagellates. J Cell Biol *34*, 345–364. 10.1083/jcb.34.1.345.
44. Marshall, W.F., and Rosenbaum, J.L. (2001). Intraflagellar transport balances continuous turnover of outer doublet microtubules : implications for flagellar length control . Journal of Cell Biology *155*, 405–414. 10.1083/jcb.200106141.
45. Auclair, W., and Siegel, B.W. (1966). Cilia Regeneration in the Sea Urchin Embryo: Evidence for a Pool of Ciliary Proteins. Science (1979) *154*.
46. Wingfield, J.L., Mengoni, I., Bomberger, H., Jiang, Y.-Y., Walsh, J.D., Brown, J.M., Picariello, T., Cochran, D.A., Zhu, B., Pan, J., et al. (2017). IFT trains in different stages

of assembly queue at the ciliary base for consecutive release into the cilium. Elife *6*, e26609. 10.7554/eLife.26609.

47. Quidwai, T., Wang, J., Hall, E.A., Petriman, N.A., Leng, W., Kiesel, P., Wells, J.N., Murphy, L.C., Keighren, M.A., Marsh, J.A., et al. (2021). A WDR35-dependent coat protein complex transports ciliary membrane cargo vesicles to cilia. Elife *10*, e69786. 10.7554/eLife.69786.

48. Hendel, N.L., Thomson, M., and Marshall, W.F. (2018). Diffusion as a Ruler: Modeling Kinesin Diffusion as a Length Sensor for Intraflagellar Transport. Biophys J *114*, 663–674. https://doi.org/10.1016/j.bpj.2017.11.3784.

49. Fai, T.G., Mohapatra, L., Kar, P., Kondev, J., and Amir, A. (2019). Length regulation of multiple flagella that self-assemble from a shared pool of components. Elife *8*, e42599. 10.7554/eLife.42599.

50. Sedzinski, J., Hannezo, E., Tu, F., Biro, M., and Wallingford, J.B. (2016). Emergence of an Apical Epithelial Cell Surface In Vivo. Dev Cell *36*, 24–35. https://doi.org/10.1016/j.devcel.2015.12.013.

51. Hibbard, J.V.K., Vázquez, N., and Wallingford, J.B. (2022). Cilia proteins getting to work – how do they commute from the cytoplasm to the base of cilia? J Cell Sci *135*, jcs259444. 10.1242/jcs.259444.

52. Conkar, D., Bayraktar, H., and Firat-Karalar, E.N. (2019). Centrosomal and ciliary targeting of CCDC66 requires cooperative action of centriolar satellites, microtubules and molecular motors. Sci Rep *9*, 14250. 10.1038/s41598-019-50530-4.

53. Conkar, D., Culfa, E., Odabasi, E., Rauniyar, N., Yates III, J.R., and Firat-Karalar, E.N. (2017). The centriolar satellite protein CCDC66 interacts with CEP290 and functions in cilium formation and trafficking. J Cell Sci *130*, 1450–1462. 10.1242/jcs.196832.

54. Khokha, M.K., Chung, C., Bustamante, E.L., Gaw, L.W.K., Trott, K.A., Yeh, J., Lim, N., Lin, J.C.Y., Taverner, N., Amaya, E., et al. (2002). Techniques and probes for the study of Xenopus tropicalis development. Developmental Dynamics *225*, 499–510. https://doi.org/10.1002/dvdy.10184.

55. Zahn, N., James-Zorn, C., Ponferrada, V.G., Adams, D.S., Grzymkowski, J., Buchholz, D.R., Nascone-Yoder, N.M., Horb, M., Moody, S.A., Vize, P.D., et al. (2022). Normal Table of Xenopus development: a new graphical resource. Development *149*, dev200356. 10.1242/dev.200356.

56. Kim, S.K., Zhang, S., Werner, M.E., Brotslaw, E.J., Mitchell, J.W., Altabbaa, M.M., and Mitchell, B.J. (2018). CLA MP/Spef1 regulates planar cell polarity signaling and asymmetric microtubule accumulation in the Xenopus ciliated epithelia. Journal of Cell Biology *217*, 1633–1641. 10.1083/jcb.201706058.

57. Werner, M.E., Mitchell, J.W., Putzbach, W., Bacon, E., Kim, S.K., and Mitchell, B.J. (2014). Radial intercalation is regulated by the par complex and the microtubule-stabilizing protein CLAMP/Spef1. Journal of Cell Biology *206*, 367–376. 10.1083/jcb.201312045.

Figure 1

A

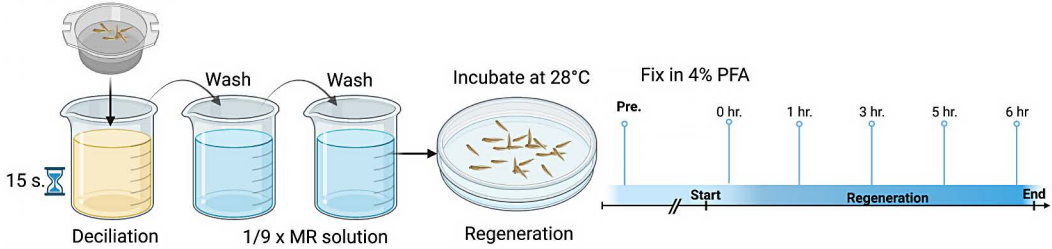
Stage 25-28 embryos
Wash
Wash
Incubate at 28°C
Fix in 4% PFA
15 s.
Deciliation
1/9 x MR solution
Regeneration
Pre.
0 hr.
1 hr.
3 hr.
5 hr.
6 hr
Start
Regeneration
End

B

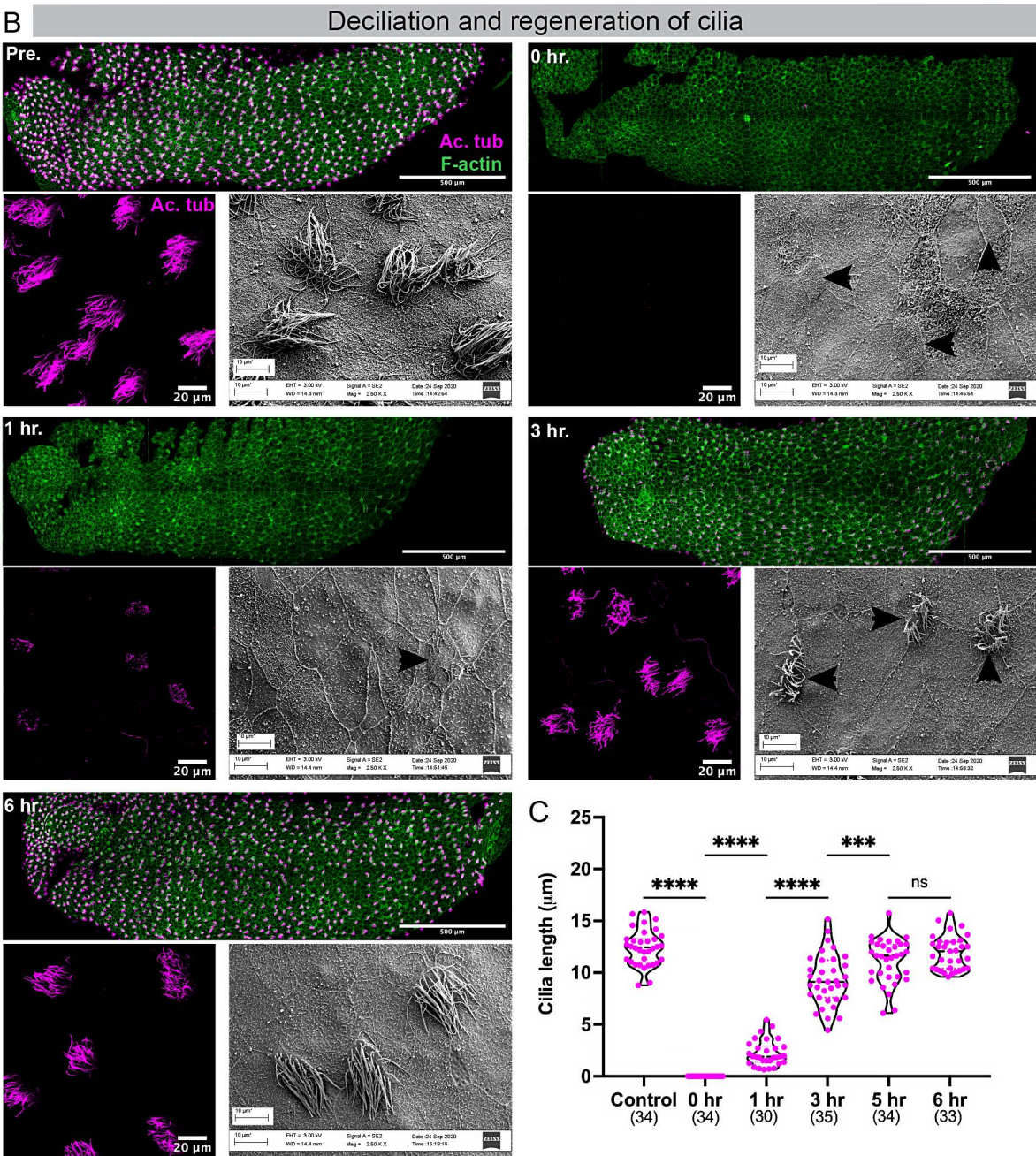
Deciliation and regeneration of cilia
Pre.
Ac. tub
F-actin
Ac. tub
0 hr.
1 hr.
3 hr.
6 hr.
20 µm
500 µm

C

Cilia length (µm)
25
20
15
10
5
0
****
****
****
***
ns
Control (34)
0 hr (34)
1 hr (30)
3 hr (35)
5 hr (34)
6 hr (33)

Figure 2

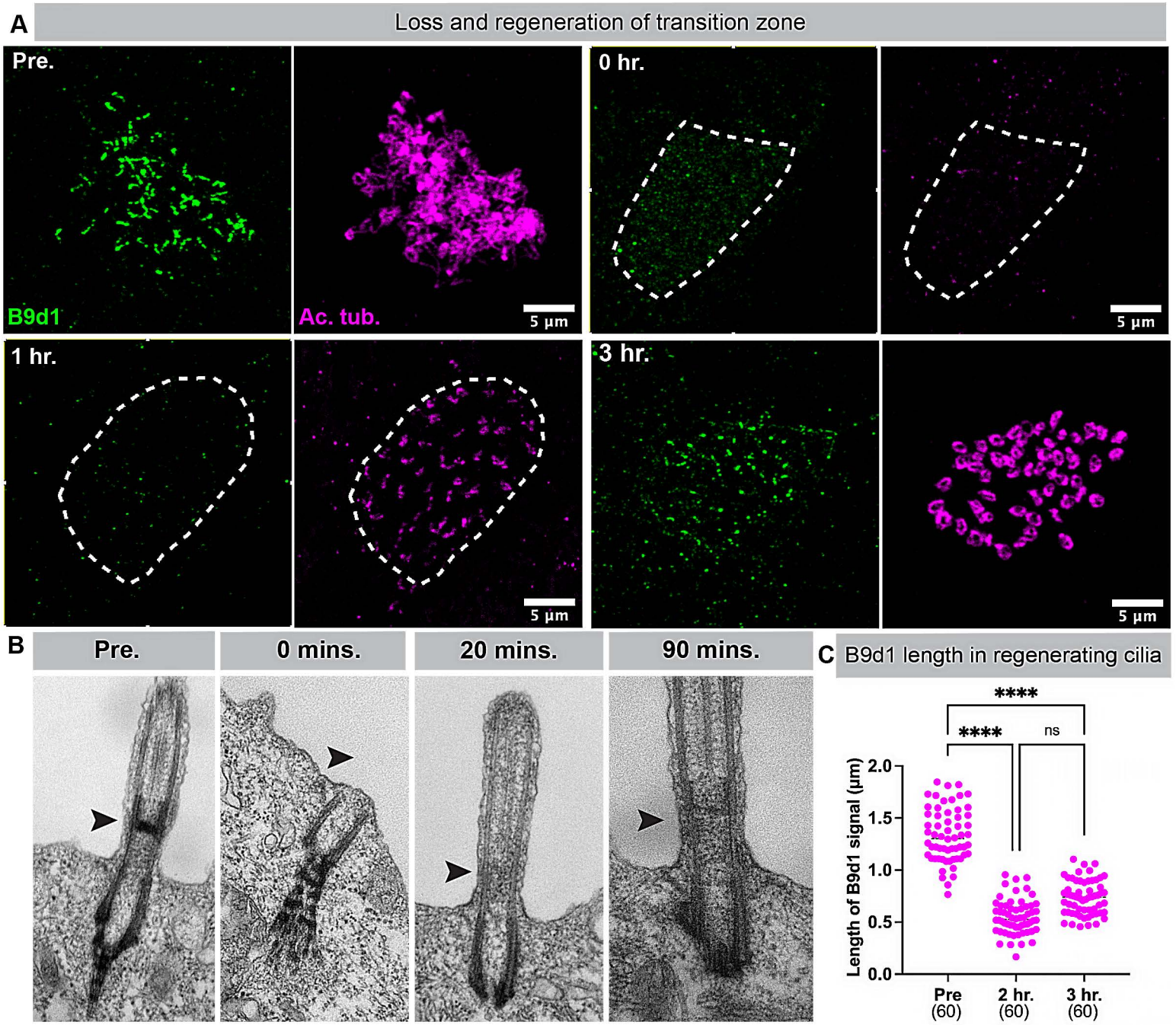
A
Loss and regeneration of transition zone
Pre.
B9d1
Ac. tub.
5 µm
0 hr.
5 µm
1 hr.
5 µm
3 hr.
5 µm
B
Pre.
0 mins.
20 mins.
90 mins.
C
B9d1 length in regenerating cilia
****
****
ns
Length of B9d1 signal (µm)
2.0
1.5
1.0
0.5
0.0
Pre (60)
2 hr. (60)
3 hr. (60)

Figure 3

A

Recovery of Sentan signal during regeneration

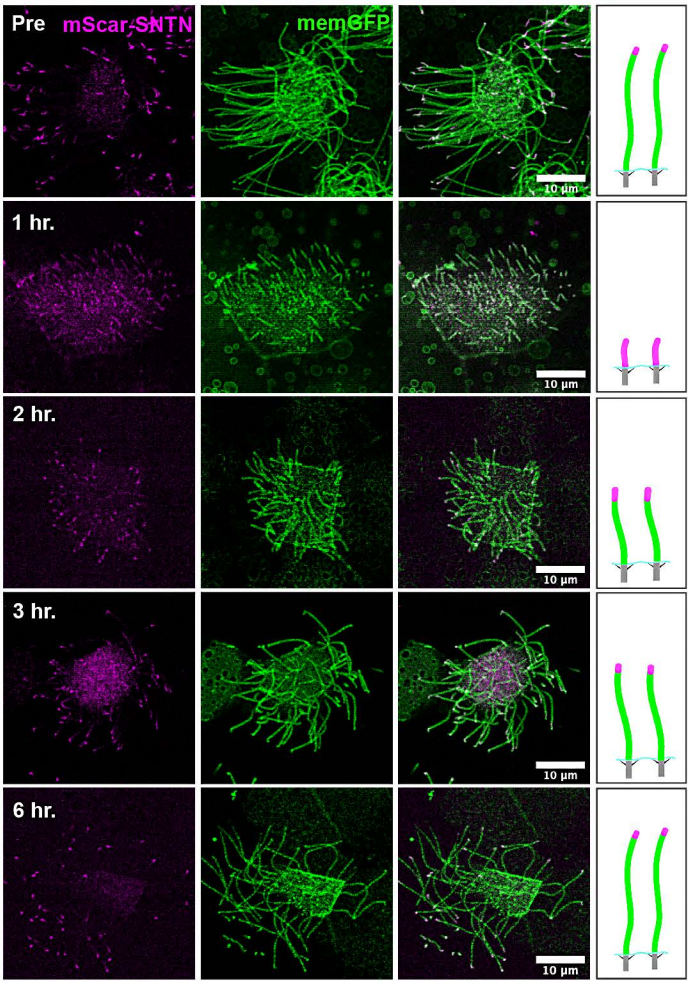

B

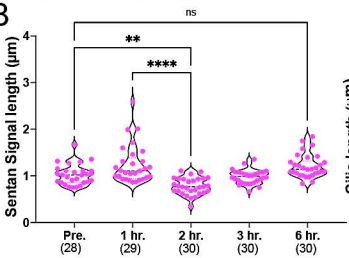

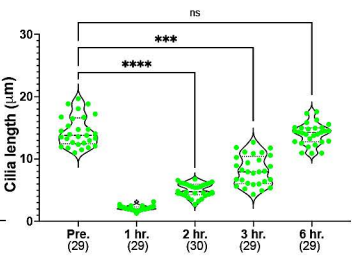

A Figure 4

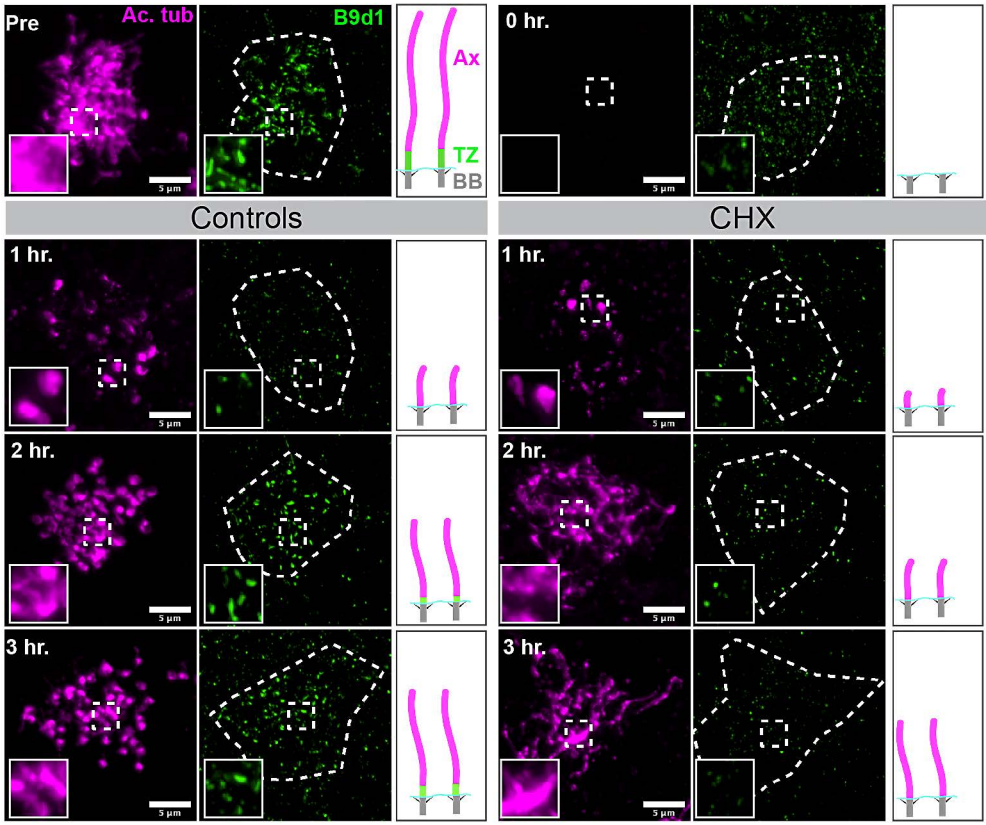
Pre
Ac. tub
B9d1
Ax
TZ
BB
0 hr.
Controls
CHX
1 hr.
2 hr.
3 hr.
5 µm

B

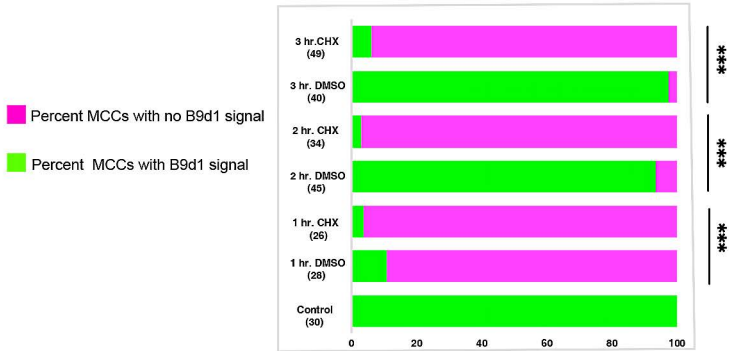
Quantification of MCCs with B9d1 signal
Percent MCCs with no B9d1 signal
Percent MCCs with B9d1 signal
3 hr.CHX (49)
3 hr. DMSO (40)
2 hr. CHX (34)
2 hr. DMSO (45)
1 hr. CHX (26)
1 hr. DMSO (28)
Control (30)
0
20
40
60
80
100
***
***
***

Figure 5

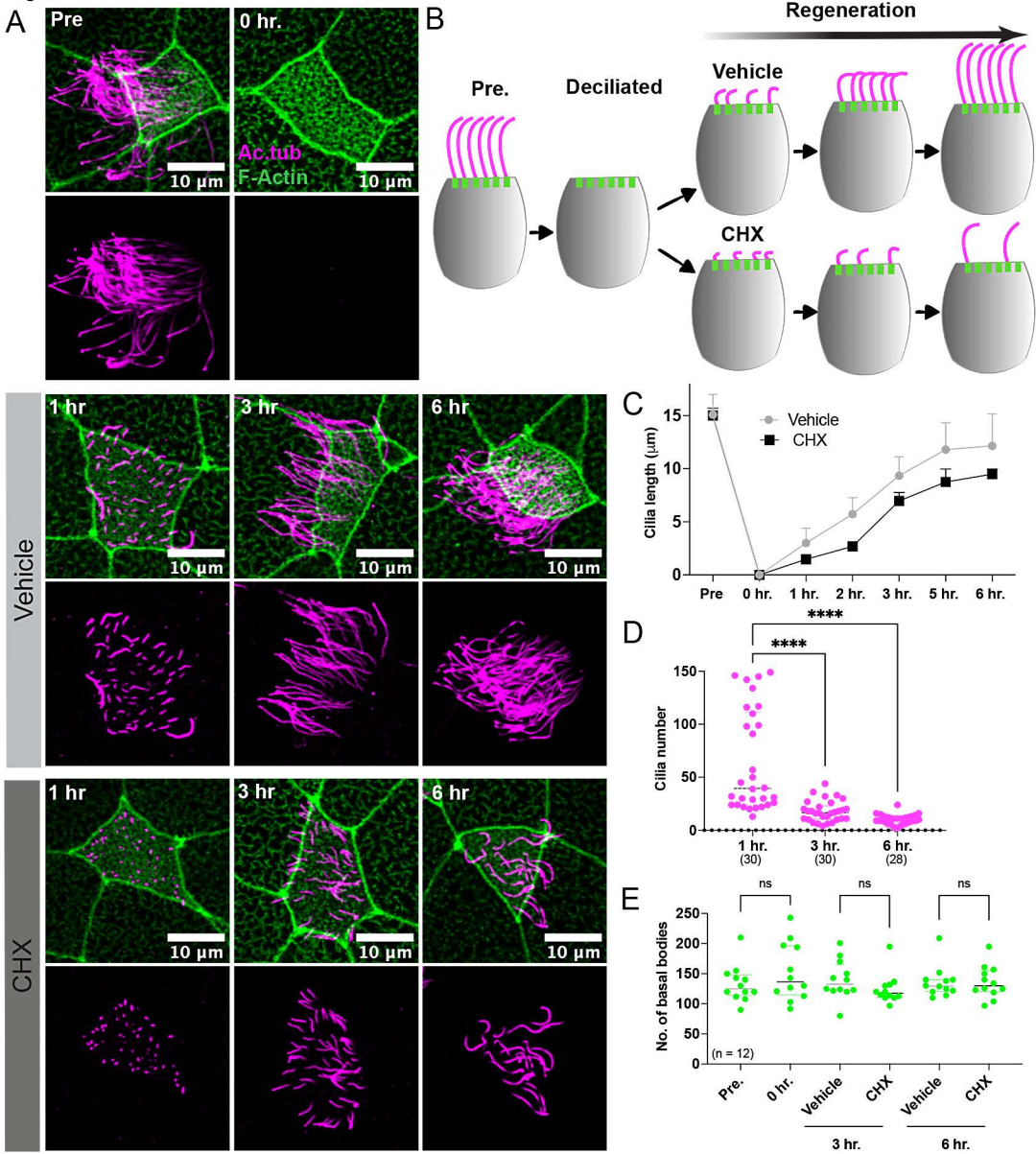
A
Pre
0 hr.
Ac.tub
F-Actin
10 µm
B
Regeneration
Pre.
Deciliated
Vehicle
CHX
Vehicle
1 hr
3 hr
6 hr
CHX
C
Vehicle
CHX
Cilia length (µm)
Pre
0 hr.
1 hr.
2 hr.
3 hr.
5 hr.
6 hr.
D
****
Cilia number
1 hr. (30)
3 hr. (30)
6 hr. (28)
E
ns
No. of basal bodies
(n = 12)
Pre.
0 hr.
Vehicle
CHX
3 hr.
6 hr.

Figure 6

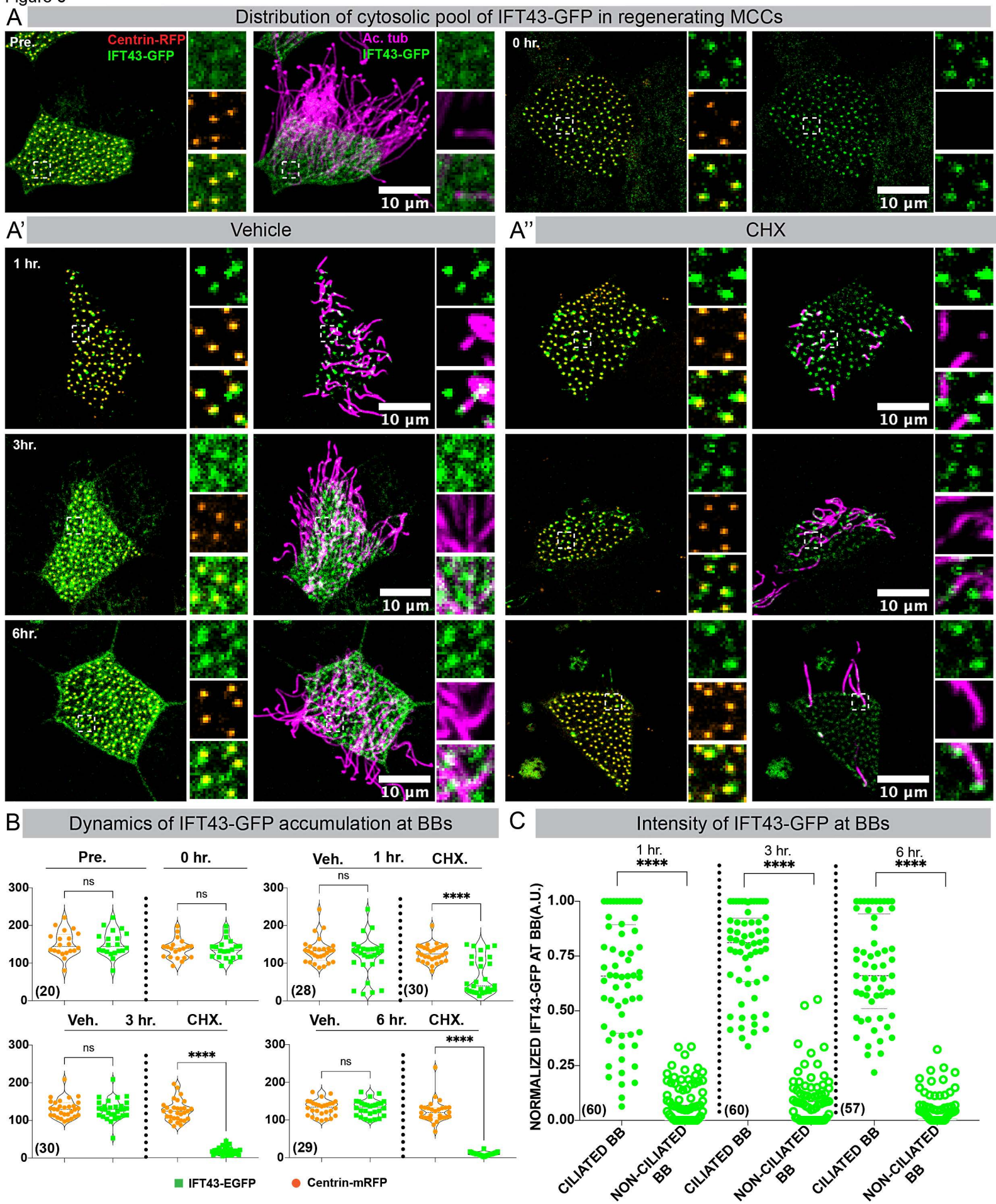
A
Distribution of cytosolic pool of IFT43-GFP in regenerating MCCs
Pre.
Centrin-RFP
IFT43-GFP
Ac. tub
IFT43-GFP
0 hr.
10 µm
A'
Vehicle
A''
CHX
1 hr.
3hr.
6hr.
B
Dynamics of IFT43-GFP accumulation at BBs
Pre.
0 hr.
Veh.
1 hr.
CHX.
3 hr.
6 hr.
ns
****
(20)
(28)
(30)
(29)
IFT43-EGFP
Centrin-mRFP
C
Intensity of IFT43-GFP at BBs
1 hr.
3 hr.
6 hr.
NORMALIZED IFT43-GFP AT BB(A.U.)
(60)
(57)
CILIATED BB
NON-CILIATED BB

Figure 7

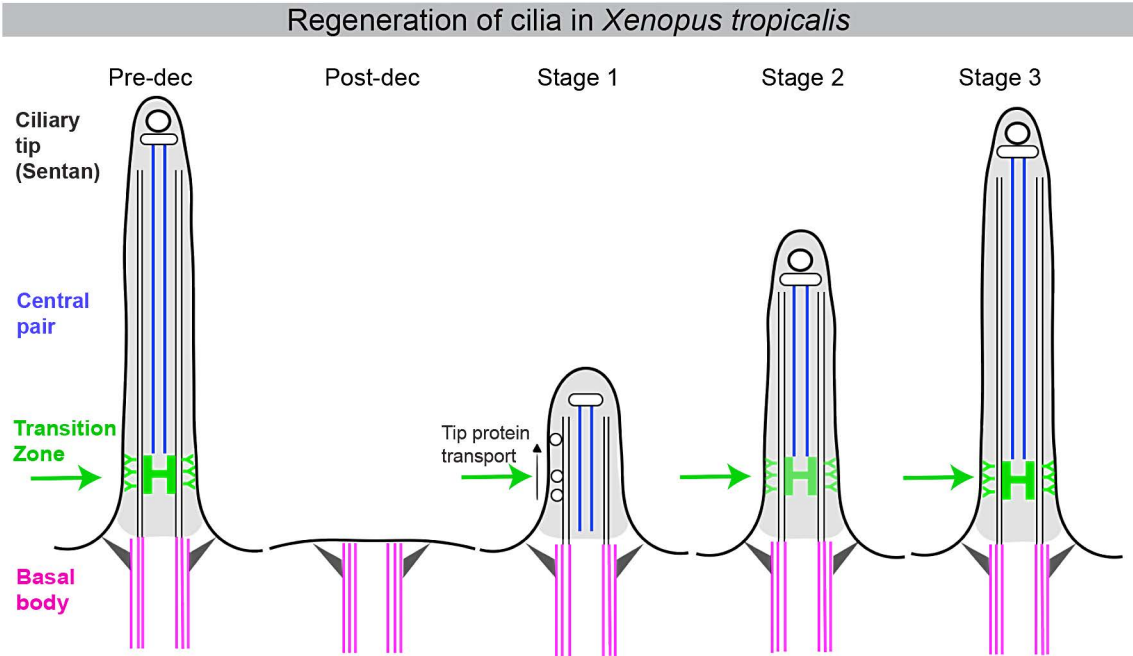
Regeneration of cilia in *Xenopus tropicalis*
Pre-dec
Post-dec
Stage 1
Stage 2
Stage 3
Ciliary tip (Sentan)
Central pair
Transition Zone
Basal body
Tip protein transport
H
H
H

Figure S1

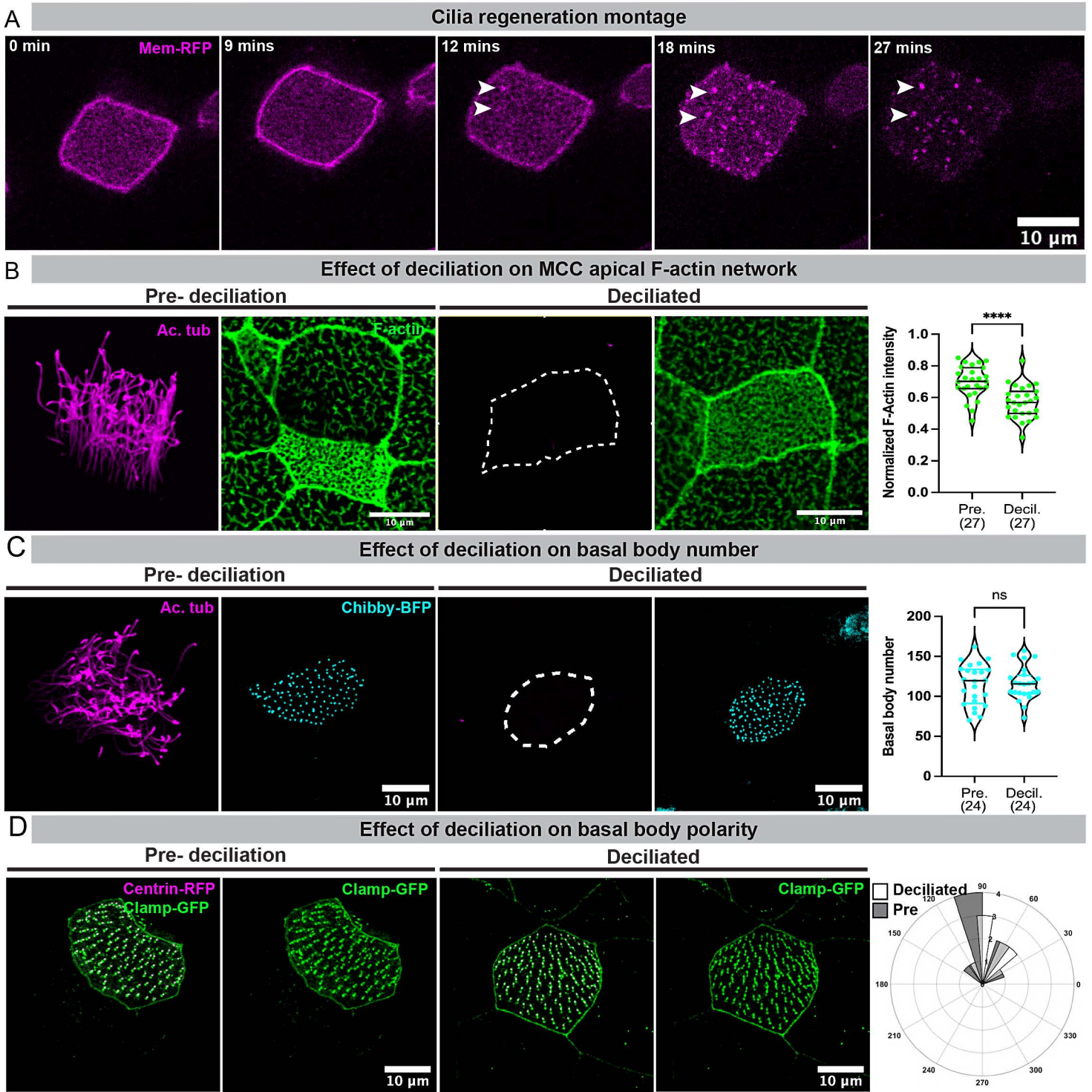
A
Cilia regeneration montage
0 min
Mem-RFP
9 mins
12 mins
18 mins
27 mins
10 µm
B
Effect of deciliation on MCC apical F-actin network
Pre- deciliation
Deciliated
Ac. tub
F-actin
10 µm
10 µm
****
Normalized F-Actin intensity
1.0
0.8
0.6
0.4
0.2
0.0
Pre. (27)
Decil. (27)
C
Effect of deciliation on basal body number
Pre- deciliation
Deciliated
Ac. tub
Chibby-BFP
10 µm
10 µm
ns
Basal body number
200
150
100
50
0
Pre. (24)
Decil. (24)
D
Effect of deciliation on basal body polarity
Pre- deciliation
Deciliated
Centrin-RFP
Clamp-GFP
Clamp-GFP
Clamp-GFP
10 µm
10 µm
Deciliated
Pre
90
60
30
0
330
300
270
240
210
180
150
120
1
2
3
4

Figure S2

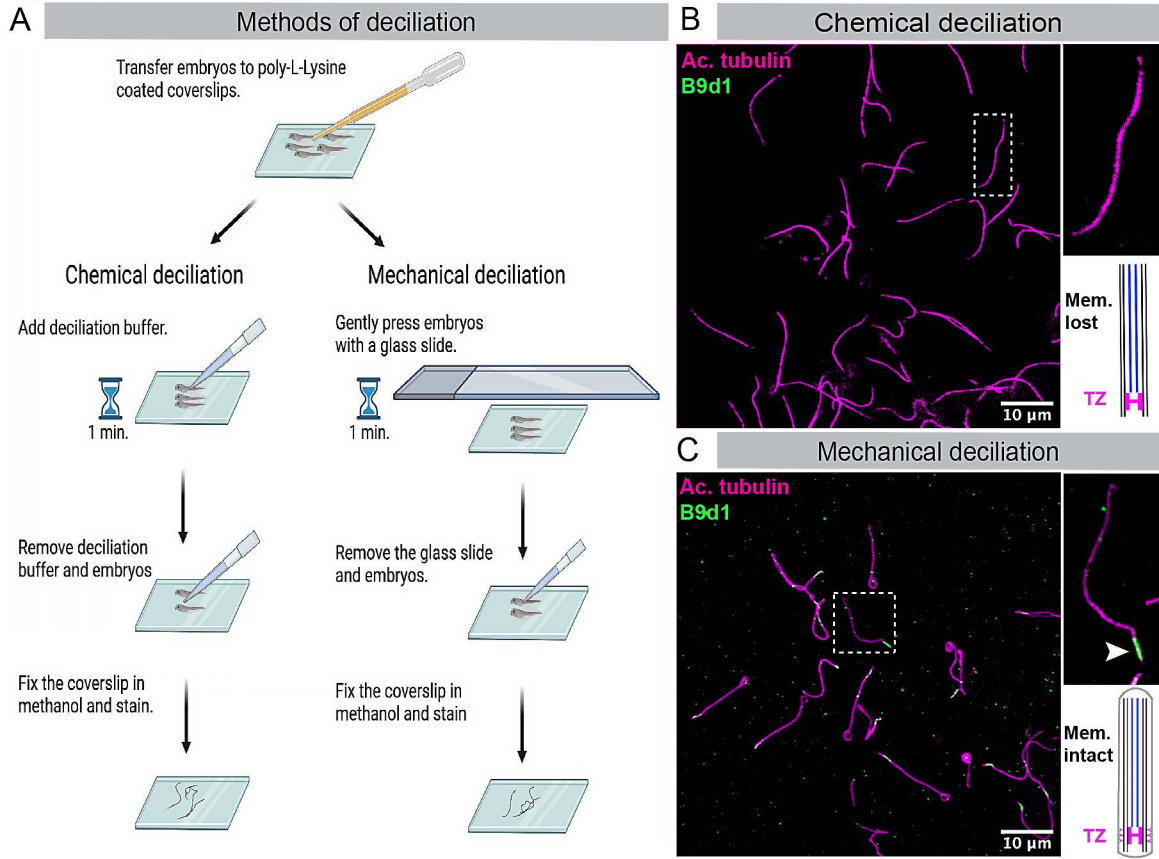
A
Methods of deciliation
Transfer embryos to poly-L-Lysine coated coverslips.
Chemical deciliation
Mechanical deciliation
Add deciliation buffer.
1 min.
Remove deciliation buffer and embryos
Fix the coverslip in methanol and stain.
Gently press embryos with a glass slide.
1 min.
Remove the glass slide and embryos.
Fix the coverslip in methanol and stain
B
Chemical deciliation
Ac. tubulin
B9d1
10 µm
Mem. lost
TZ
H
C
Mechanical deciliation
Ac. tubulin
B9d1
10 µm
Mem. intact
TZ
H

Figure S3

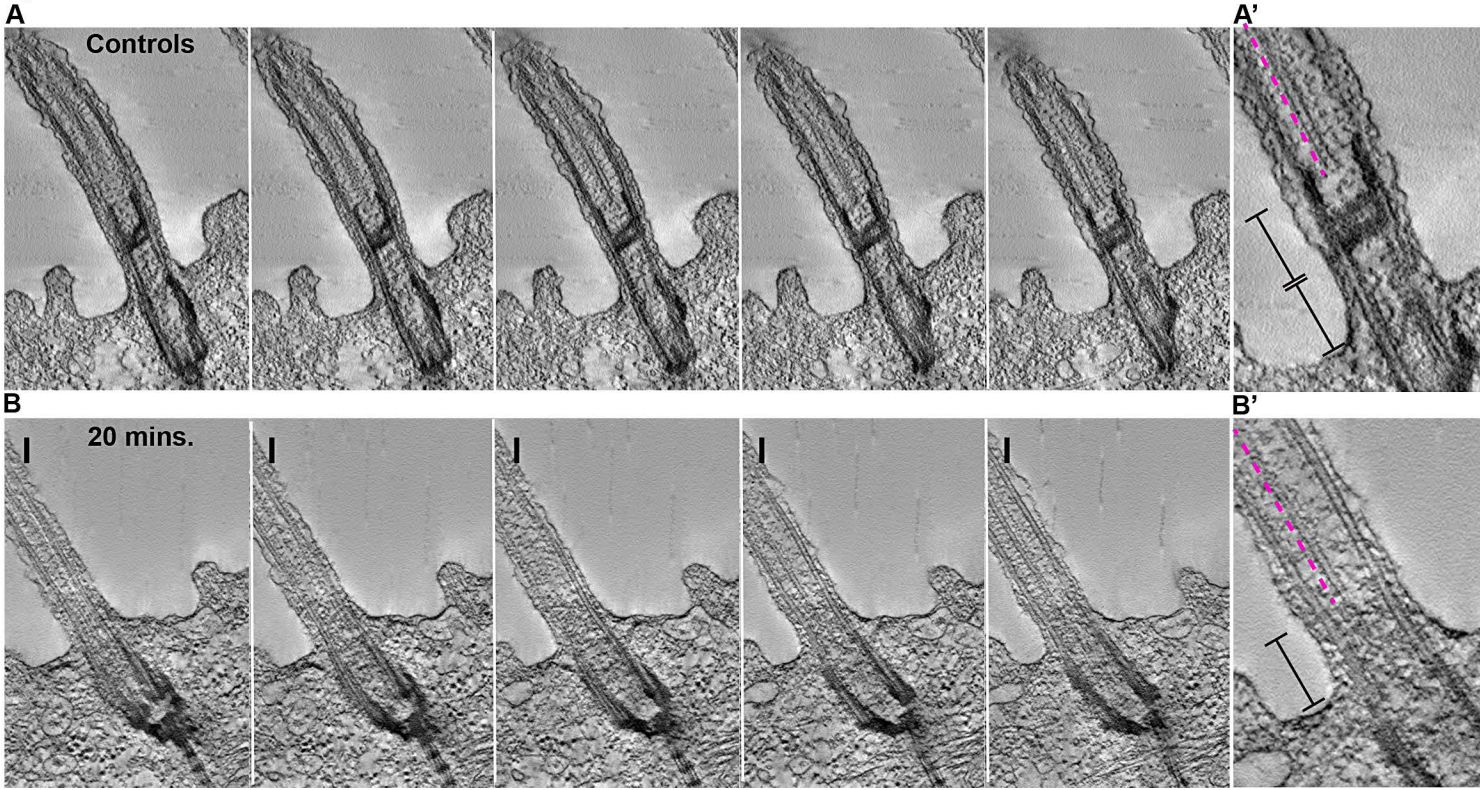

Figure S4

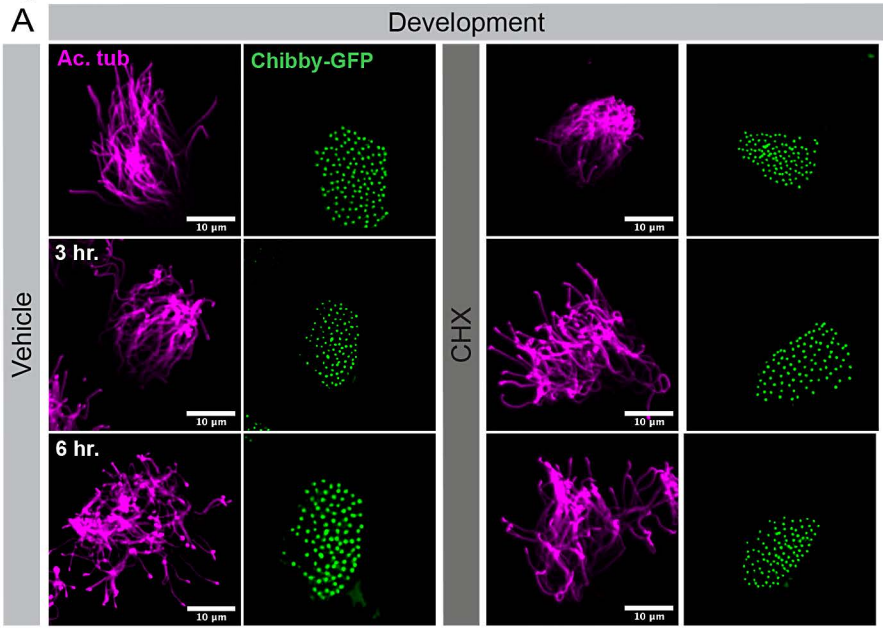
A
Development
Ac. tub
Chibby-GFP
Vehicle
CHX
3 hr.
6 hr.
10 µm

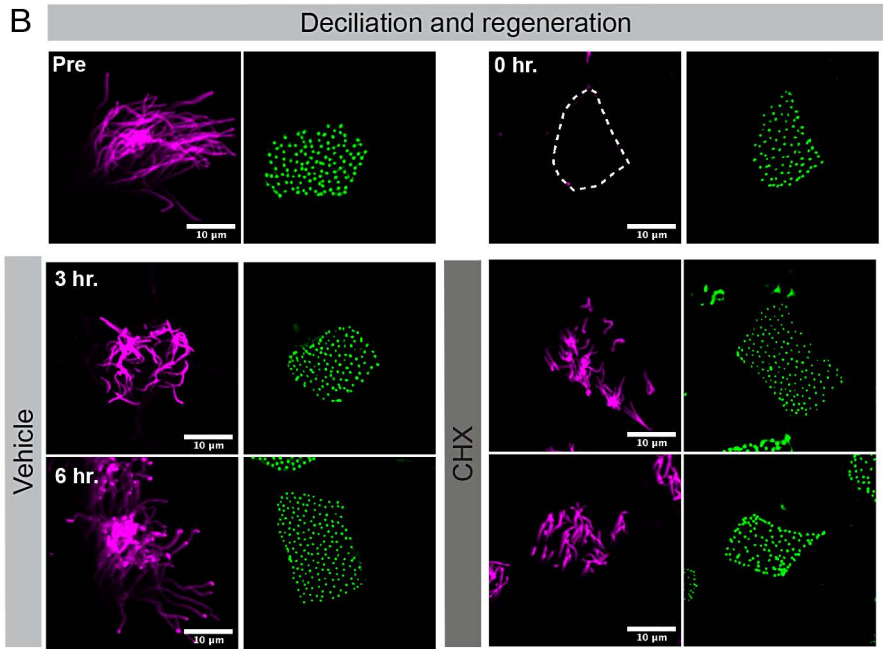
B
Deciliation and regeneration
Pre
0 hr.
3 hr.
6 hr.
Vehicle
CHX
10 µm